

# Bioactive glass-biopolymers-gold nanoparticle based composites for tissue engineering applications

Alexandra Dreanca<sup>a,b</sup>, Marieta Muresan-Pop<sup>a</sup>, Marian Taulescu<sup>b,\*</sup>, Zsejke-Réka Tóth<sup>a,c</sup>,  
Sidonia Bogdan<sup>b</sup>, Cosmin Pestean<sup>b</sup>, Stephie Oren<sup>b</sup>, Corina Toma<sup>b</sup>, Andra Popescu<sup>b</sup>,  
Emőke Páll<sup>b</sup>, Bogdan Sevastre<sup>b</sup>, Lucian Baia<sup>a,d</sup>, Klara Magyari<sup>a,e,\*\*</sup>

<sup>a</sup> Nanostructured Materials and Bio-Nano-Interfaces Center, Interdisciplinary Research Institute on Bio-Nano-Sciences, Babes-Bolyai University, T. Laurian 42, 400271 Cluj-Napoca, Romania

<sup>b</sup> Faculty of Veterinary Medicine, University of Agricultural Science and Veterinary Medicine, 3-5 Calea Manastur, 400372 Cluj-Napoca, Romania

<sup>c</sup> Research Group of Environmental Chemistry, Department of Applied and Environmental Chemistry, Institute of Chemistry, University of Szeged, Rerrich B. sq. 1., 6720 Szeged, Hungary

<sup>d</sup> Faculty of Physics, Babes-Bolyai University, M. Kogalniceanu 1, 400084 Cluj-Napoca, Romania

<sup>e</sup> Institute of Environmental Science and Technology, University of Szeged, Tisza Lajos blvd. 103, 6720 Szeged, Hungary

## ARTICLE INFO

### Keywords:

Alginate  
Pullulan  
Silicate glasses  
Gold nanoparticles

## ABSTRACT

Biomaterials based on bioactive glass with gold nanoparticle composites have many applications in tissue engineering due to their tissue regeneration and angiogenesis capacities. The objectives of the study were to develop new composites using bioactive glass with gold nanospheres (BGAuSP) and gold nanocages (BGAuND), individually introduced in alginate-pullulan (Alg-Pil) polymer, to evaluate their biocompatibility potential, and to compare the obtained results with those achieved when  $\beta$ -tricalcium phosphate-hydroxyapatite ( $\beta$ TCP/HA) replaced the BG. The novel composites underwent structural and morphological characterization followed by *in vitro* viability testing on fibroblast and osteoblast cell lines. Additionally, the biomaterials were subcutaneously implanted in Sprague Dawley rats, for *in vivo* biocompatibility assessment during 3 separate time frames (14, 30 and 60 days). The biological effects were evaluated by histopathology and immunohistochemistry. The physical characterization revealed the cross-linking between polymers and glasses/ceramics and demonstrated a suitable thermal stability for sterilization processes. The *in vitro* assays demonstrated adequate form, pore size of composites ranging from few micrometers up to 100  $\mu$ m, while the self-assembled apatite layer formed after simulated body fluid immersion confirmed the composites' bioactivity. Viability assays have highlighted optimal cellular proliferation and *in vitro* biocompatibility for all tested composites. Furthermore, based on the *in vivo* subcutaneous analyses the polymer composites with BGAuNP have shown excellent biocompatibility at 14, 30 and 60 days, exhibiting marked angiogenesis while, tissue proliferation was confirmed by high number of Vimentin positive cells, in comparison with the polymer composite that contains  $\beta$ TCP/HA, which induced an inflammatory response represented by a foreign body reaction. The obtained results suggest promising, innovative, and biocompatible composites with bioactive properties for future soft tissue and bone engineering endeavours.

## 1. Introduction

Novel biomaterials based on bioactive glasses (BG) with metal nanoparticle composites have received much attention in the last few years [1–4]. The focus has been directed to biomedical applications in

tissue engineering [5–7]. Gold nanoparticles (AuNPs) are attracting considerable interest due to their supportive effects in growth and proliferation of the living cells, thus solidifying a major role in the regeneration of damaged and diseased tissues [8,9]. As well, significant efforts are made to ensure the biocompatibility and bioactivity of mixed

\* Corresponding author.

\*\* Correspondence to: K. Magyari, Nanostructured Materials and Bio-Nano-Interfaces Center, Interdisciplinary Research Institute on Bio-Nano-Sciences, Babes-Bolyai University, T. Laurian 42, 400271 Cluj-Napoca, Romania.

E-mail addresses: [marian.taulescu@usamvcluj.ro](mailto:marian.taulescu@usamvcluj.ro) (M. Taulescu), [klara.magyari@ubbcluj.ro](mailto:klara.magyari@ubbcluj.ro) (K. Magyari).

<https://doi.org/10.1016/j.msec.2021.112006>

Received 14 September 2020; Received in revised form 29 January 2021; Accepted 23 February 2021

Available online 3 March 2021

0928-4931/© 2021 Elsevier B.V. All rights reserved.

composites at the place of injury, at the same time having a minimal systemic immune response [10]. Besides this, other promising properties such as surface modification, good stability, optical properties and antibacterial effects could be targeted or exploited [11].

Previous studies have shown that various biopolymer composites have the ability to stimulate the regenerative capacity of a targeted tissue [12]. The advantage of using such products is that the composites are biocompatible, biodegradable and non-toxic [13]. Considering these properties, in this study, two natural polymers, alginate and pullulan, were chosen due to their additional non-mutagenic and non-carcinogenic characteristics [14].

A growing body of literature has examined alginate and pullulan properties; alginate, a biodegradable natural polysaccharide, having a good scaffold-forming property. Alginate is composed of guluronic acid and mannuronic acid thus, considered biocompatible and also, can be easily modified into any form such as hydrogels, microspheres, sponges, foams, fibers and microcapsules [13,15]. Physical and chemical modification can be performed by combining alginate with other molecules, having excellent porosity (>microns), biodegradability, mechanical strength, which is equivalent to cortical bone, being able to fill irregularly shaped defects and release bioactive molecules at the site of injury [15]. The missing properties of alginate appear in bioactivity and cell adhesion which limit their application in bone tissue engineering.

The pullulan is a water-soluble neutral polysaccharide used in numerous application in food and pharmaceutical industry [16–19]. Their beneficial properties such as hamo- and biocompatible, high hydration capacity indicate their applicability in tissue engineering [18]. Having the multiple functional groups they allow the crosslinking, delivery of cells and biomolecules and provide exclusive bioactive properties [14,19,20]. The limit in applicability of pullulan in tissue engineering is due to inability to deliver a surface that supports cell adhesion and diffusion [18]. The alginate-pullulan composites have already demonstrated the good bioactivity and *in vivo* qualities, in terms of bone regeneration [21,22].

Furthermore, in order to enhance composite bone bonding abilities properties, such as osteoconductibility and bioactivity, silicate-based BG were used. These silicate BG were already shown to promote regeneration on both hard and soft tissue structures [22–24]. Their main activity is to bond soft and hard tissues through the carbonate hydroxyapatite layer that is formed when exposed to biological fluid [25]. The cytotoxic effects of silicate-based BG have already been tested in previous articles, and the results demonstrated that the glass samples presented very good *in vitro* tolerance affirming biocompatibility as well as a lack of toxicity [2,24,26]. The viability of keratinocytes, in the presence of the BG, was very close to or greater than 100%, thus highlighting the non-toxic effects of the glass alongside the positive proliferative effects [26]. Bioactive glass has already been proven to enhance bone regeneration and osteointegration, as was established in a study that used nanostructured porous silica coated titanium rods in bone engineering, to improve clinical outcomes of titanium rod implantation [27].

AuNPs have attracted scientific and technological interest due to their unique physical and chemical properties. They have numerous biomedical applications, such as bio imaging, drug delivery, cancer therapy and diagnostic potential [28].

Vieira et al. [29] emphasizes the use of gold metallic nanoparticles embedded in scaffolds used in bone regeneration, due to their potential of promoting bone cell differentiation, statement enforced by Zhang et al. [30]. Moreover, previous work was focused on developing the perfect scaffold with bioactive molecules such as AuNPs, which were found not only able to improve the scaffolds structure, but they also guide cellular behaviour [31].

Our previous studies have demonstrated that embedding spherical AuNPs (AuSP) into the bioactive glass matrix, biocompatibility and bioactive biomaterials were obtained [2,26]. These materials exhibited excellent proliferation rates in human keratinocyte cells. Encouraged by these findings spherical gold nanocages (AuIND) were introduced into

the silicate glass matrices by means of the sol-gel derived method [26]. Due to the silver content these composites revealed not only antibacterial effects against *Pseudomonas aeruginosa*, but also *in vitro* biocompatibility on the same keratinocyte cellular line.

The main objective of the present study was to develop new composites for future tissue engineering applications in bone regeneration, using bioactive glass with gold nanoparticles (BGAuNPs) introduced in alginate-pullulan polymer composites (Alg-Pll). For this purpose, we based on the reported findings in which BG-gold nanospheres (BGAuSP) and BG-gold nanocages (BGAuIND) composites were used [2,24,26]. Although the BGAuIND has similar *in vitro* biocompatibility performance to those of the BGAuSP, their small amount of silver content can affect both *in vivo* biocompatibility and organ toxicity. The first step was the structural and morphological characterization, followed by *in vitro* bioactivity and *in vitro* biocompatibility studies on osteoblasts and fibroblast cells. Additionally, *in vivo* assays were performed on Sprague-Dawley rats together with sub-acute organ (liver and kidney) toxicity, subcutaneous biocompatibility analyses, and followed by the assessment of the soft tissue regeneration potential by histopathology and immunohistochemistry. For the control  $\beta$ -tricalcium phosphate-hydroxyapatite ( $\beta$ TCP/HA) was used after introducing it in an alginate-pullulan composite. It is known that composites with  $\beta$ TCP/HA improved new bone formation in the rat calvarial defect model, suggesting its application as a bone graft [32]. In another study, compounds using collagen-hydroxyapatite scaffolds were found to induce differentiation towards osteogenic and chondrogenic lineage *in vitro* and induced bone augmentation and angiogenesis after ectopic implantation, *in vivo* [33].

## 2. Materials and methods

### 2.1. Materials

All chemicals were used as received without further purification. The precursors used for the glass synthesis were tetraethyl orthosilicate (TEOS,  $\geq 99\%$ , Merck), triethyl phosphate (TEP,  $\geq 99\%$ , Merck) and calcium nitrate tetrahydrate ( $\text{Ca}(\text{NO}_3)_2 \cdot 4\text{H}_2\text{O}$ ,  $\geq 99\%$ , Lach-Ner), hydrolysed in presence of nitric acid ( $\text{HNO}_3$ , 65%). Hydrogen tetrachloroaurate (III) hydrate ( $\text{HAuCl}_4 \cdot 3\text{H}_2\text{O}$ , 99.99%, Sigma-Aldrich), trisodium citrate dihydrate (ACS, 99.0%), sodium borohydride ( $\text{NaBH}_4$ , purum  $\geq 96\%$ , Sigma-Aldrich), Pluronic F127 (powder, BioReagent, suitable for cell, Sigma-Aldrich) were used to AuNPs synthesis. Ultrapure water and absolute ethanol were used throughout the whole experimental process. For control samples powder  $\beta$ TCP/HA-60%-40% were used from Botiss Biomaterials. Sodium alginate and pullulan (from Aureobasidium pullulans) polymeric powder were obtained from Sigma-Aldrich.

### 2.2. BG synthesis and characterization

The  $60\text{SiO}_2 \cdot 31.85\text{CaO} \cdot 8\text{P}_2\text{O}_5 \cdot 0.15\text{Au}_2\text{O}$  (mol%) glass samples (the gold amount is conventionally indicated in the oxidic form  $\text{Au}_2\text{O}$ ) with spherical gold nanoparticle (BGAuSP) or with spherical gold nanocages (BGAuIND) were prepared by sol-gel method as described elsewhere [2,26]. This amount of gold introduced into the glass matrices represents the 0.9 at% in BGAuSP and 0.89 at% in BGAuIND, respectively. The silver content in the BGAuIND is approx. 0.0024 at%. The spherical nanoparticles (AuSP) were obtained using the Turkevich-Frens method [34] using  $\text{HAuCl}_4 \cdot 3\text{H}_2\text{O}$  ( $10^{-3}$  M) solution. The solution was heated until the boiling point of water and afterwards, trisodium citrate ( $38.8 \cdot 10^{-3}$  M) solution was instantly added to the boiling gold precursor solution using a 10:1 volume ratio. The whole procedure continued for 30 min and then it was cooled to room temperature. Gold nanocages (AuIND) were prepared by adapting a well-known method in the literature [35,36]. In 130 mL of deionized  $\text{H}_2\text{O}$ , 18.9 mL 2.31 mM trisodium citrate ( $\text{Na}_3\text{C}_6\text{H}_5\text{O}_7$ ) was introduced under constant

homogenization. After 30 min of stirring, 1.65 mL AgNO<sub>3</sub> (83.7 mM) was added. As the reductant NaBH<sub>4</sub> solution (3 mL, 0.55 M) was applied in excess, which was pre-cooled at 5 °C. The suspension was stirred for an additional hour. The obtained solution with silver nanoparticles was heated to 100 °C and refluxed for 10 min. 1.8 mL, 25.39 mM chloroauric acid was added subsequently to the reaction mixture and it was maintained for 20 min at 100 °C. After cooling the reaction mixture to room temperature, an excess amount of powdered NaCl was added into the solution, to eliminate the remaining Ag<sup>+</sup> in form of AgCl.

The AuNPs were stabilized using a Pluronic F127 block copolymer solution of  $0.5 \times 10^{-3}$  M. The solution containing the AuNPs was stirred for 20 min, followed by an aging process of 24 h to assure the adherence of the polymer molecules. The excess of Pluronic F127 was removed by collecting the supernatant liquid from the centrifugation tubes, which were held for 30 min at 12,000 rpm.

For the glass samples, the reactants were added consecutively after 1-h intervals, under continuous stirring. Finally, there were added the solution of colloidal AuNPs, which was stirred 1 h. The gelation was achieved in 2 days at 37 °C, after that the as-prepared gels were aged 3 days at 37 °C and afterwards dried at 120 °C for 24 h and thermally treated at 500 °C for 3 h. The AuNPs size and shape were verified using transmission electron microscope (TEM, Philips CM 10 instrument, Amsterdam, Netherlands), operating at an accelerating voltage of 200 kV. The elemental composition on the samples' surfaces was determined using X-Ray photoelectron spectroscopy (XPS, SPECS PHOIBOS 150 MCD system) employing a monochromatic Al-K<sub>α</sub> source (1486.6 eV), a hemispherical analyser and charge neutralization device. Samples were fixed on a double-sided carbon tape and care was taken to ensure that the sample particles covered the tape. Experiments were performed by operating the X-ray source with a power of 200 W, while the pressure in the analyse chamber was in the range of  $10^{-9}$ – $10^{-10}$  mbar. The binding energy scale was charge referenced to the C1s at 284.6 eV. Elemental composition was determined from survey spectra acquired at pass energy of 60 eV.

All analyses were performed on powder samples, which were milled by hand using Agate mortar. The glass samples granulation was similar. As a control samples commercial βTCP/HA with a 60%/40% ratio was used.

### 2.3. Composite synthesis

To obtain the scaffolds, the polymeric solutions of 4% (w/v), the sodium alginate and pullulan powders were dissolved in 80 °C ultrapure water at continuous stirring. For the uniform particle size, the bioactive materials were ultrasonicated for 1 h. In order to make the sodium alginate-pullulan mixture, a weight ratio of 1:0.75 was chosen, according to other reported studies [17,21,22,37]. The bioactive materials were added in the polymeric mixture in a weight ratio of 12.5 wt%. For the better dispersion bioactive materials-polymeric mixture were gently vortexed few minutes to promote the homogeneous distribution of bioactive materials within the polymer's solution. Following mixing, the composites were cast in a 96-well plate and refrigerated at 4 °C for 4 h. The plates were frozen at −18 °C for 24 h and then were lyophilized in Vacuum Freeze Dryer (BK -FD 10 Series, Biobase Biodustry, Shandong Co., Ltd) for 24 h. The composite materials were cross linked in 4% CaCl<sub>2</sub> solution for 4 h.

### 2.4. Particles size analysis

The particle size distribution of glass/ceramic materials were measured using dynamic light scattering (DLS, Malvern Instrument Zetaiser Nano-ZS) at 25 °C. The results were averaged from three measurements.

### 2.5. Structure and thermal stability analysis

The structural analyses of the obtained polymeric scaffolds were performed using FT-IR spectroscopy and the thermal stability with thermogravimetric analysis. The FT-IR absorption spectra were recorded in reflection configuration with a Jasco 6200 (Jasco, Tokyo, Japan) spectrometer, at room temperature, in the range 400–4000 cm<sup>−1</sup>; spectral resolution of 4 cm<sup>−1</sup>; using the well-known KBr pellet technique.

The thermogravimetric analysis was performed with the Shimadzu DTG-60H instrument which recorded the DTA curves as the difference between the temperature of the sample to be analysed and the alumina standard sample, and the TG curves as a change in the weight of the sample depending on the temperature. The samples were placed in alumina crucibles with a diameter of 6 mm and a height of 2.5 mm. The samples were heated from ambient temperature to 1100 °C in a mixture of 70 mL of N<sub>2</sub> at a heating rate of 10 °C min<sup>−1</sup>.

### 2.6. Porosity and morphological analysis

The glass and ceramic samples' specific surface area and pore volume were obtained from N<sub>2</sub>-adsorption-desorption isotherms, using BELCAT-A apparatus. The specific surface area was obtained by the Brunauer-Emmett-Teller (BET) method, while the pore volumes were determined by the Barret-Joyner-Halenda (BJH).

The morphology of the obtained scaffolds was analysed via a scanning electron microscopy (SEM) recording on a Hitachi S-4700 Type II cold field emission scanning electron microscope (Tokyo, Japan) equipped with Röntec QX2-EDS spectrometer operating at an acceleration voltage of 10 kV.

### 2.7. In vitro biodegradation and bioactivity assay

Degradation tests were analysed using the weight loss in simulated body fluid (SBF, pH 7.4). The samples were incubated at 37 °C for 1, 3, 7, 14 and 42 days and the SBF was replaced every 7 days. The surface of the composites per volume of SBF used was 40 mm<sup>2</sup>·mL<sup>−1</sup>. After the incubation days, samples were rinsed with distilled water, surface wiped and weighted to obtain their wet weights (W<sub>w</sub>). Then, they were dried at 37 °C for 48 h till constant weight was achieved and they were weighed to obtain their dry weights (W<sub>d</sub>). The percentage of weight lost was calculated according to the following formula:

$$\text{Weight loss\%} = \left[ \frac{W_i - W_d}{W_i} \right] \times 100 \quad (1)$$

where, W<sub>i</sub> is the initial weight of each sample.

The percentage of water absorption was calculated by using formula:

$$\text{Water absorption\%} = \left[ \frac{W_w - W_d}{W_d} \right] \times 100 \quad (2)$$

All measurements were repeated three time (see Section 2.11).

In order to evaluate the presence of apatite layer formed on samples surface after immersion in SBF, FT-IR spectra and SEM micrograph were achieved with the same equipment described above. X-ray diffraction (XRD) measurements were performed to evaluate the apatite crystalline phases formed during the immersion, by using a Shimadzu XRD 6000 diffractometer (Kyoto, Japan) using CuK<sub>α</sub> radiation ( $\lambda = 1.54 \text{ \AA}$ ) with Ni filter. The diffractograms were recorded in 2θ range from 10° to 80° with a speed 2°/min.

### 2.8. Cell viability

Cytotoxicity assays were conducted using human fibroblastic (HS 27) (ATCC 94041901) cell lines and human osteoblastic cells isolated from the patella, generous gift of Tomuleasa et al. [38]. A concentration



of  $1 \times 10^5$  cells/well was used for each of the cell lines. HS cells were cultured in DMEM (Sigma-Aldrich) supplemented with 10% fetal calf serum (FCS) (Gibco), 2 mM L-Glutamine (Sigma-Aldrich), 1% antibiotic-antimycoti (Sigma-Aldrich), and for human osteoblast cells, DMEM/F-12 (Sigma-Aldrich) with 20% FCS, 2 mM L-Glutamine, 1% antibiotics (Sigma-Aldrich), 1% non-essential amino acids (NEA) (Sigma-Aldrich) were used. Cultures were incubated at 37 °C in the presence of 5% CO<sub>2</sub> atmosphere (ATM). After 24 h, composites were placed in hanging inserts (Millicell-® TM, Millipore, Merck KGaA, Darmstadt, Germany) (0.4 µm) introduced in 24-well cell culture plates (CytoOne, Cell Culture, Mineapolis, USA) with  $1 \times 10^5$  cells/well. Wells without inserts and composites were used as controls. A secondary positive control consisting of Alg-PII polymer was used. After 24 h, the culture medium and the inserts with composites were removed from wells and 100 µL of 1 mg·mL<sup>-1</sup> MTT solution (Sigma-Aldrich) was added. After 4 h of incubation at 37 °C in the dark, the MTT solution was removed from each well and 150 µL DMSO (dimethyl sulfoxide) dye solution (Fluka, Buchs,

Switzerland) was added. The optical density of the chromogenic reaction was evaluated at 450 nm using BioTek Synergy 2 microplate reader (Winooski, VT, USA). The cell morphology (qualitative examination) was examined using light microscopy, Nikon Eclipse E 100 microscope with a DS-2Mv-L2 digital camera (Nikon Instruments, Shanghai, China).

## 2.9. In vivo biocompatibility

The composites were implanted subcutaneously in 45 males, Sprague Dawley rats. The animals were obtained from an authorized breeding unit (Cantacuzino Institute) and were housed according to ISO 10993-2 standards [39] and Directive 63/2010/EU in individual ventilated cages, at  $25 \pm 2$  °C and  $55\% \pm 10\%$  relative humidity, under a 12 h light-dark cycle, in the authorized Laboratory Animal Establishment (University of Agricultural Sciences and Veterinary Medicine Cluj-Napoca). Standard rodent diet and water *ad libitum* were provided. All animal procedures were approved by the Regional Sanitary Veterinary and

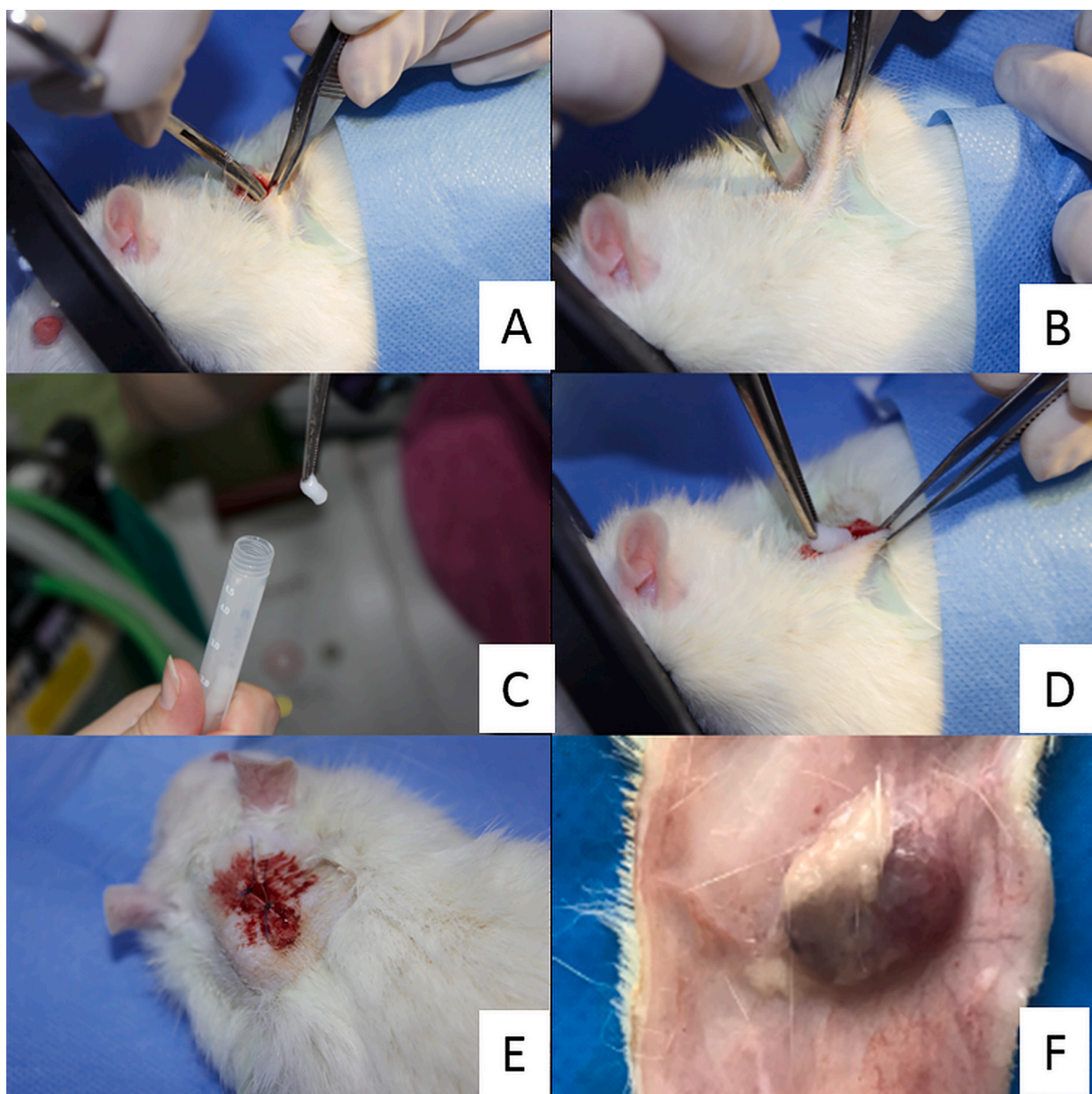


**Fig. 1.** The subcutaneous implantation of scaffold biomaterials was performed on the dorsal scapular area of the Sprague Dawley rats: small skin incision of 8–10 mm (A and B), the sterile biomaterial (C), implantation of the composite (D), post-surgical sutured skin (E) and macroscopic evaluation of the composites after 14 days (F).



Food Safety Authority (no. 173/18.07.2019) and followed the guidelines of Directive 63/2010 and national law no. 43/2014. Surgical procedures were performed according to ISO 10993-6 [40]. The surgery was performed under general anesthesia with Xylazine (6 mg/kg, Bioveta, Romania), Ketamine (60 mg/kg, Bioveta, Romania) and maintenance isoflurane 2%/oxygen 100%. The implants were placed in a pocket, under dermal tissue, in the cervical region (Fig. 1).

The animals were closely monitored during the entire duration of the study, focusing on infection prevention, using Enrofloxacin (5 mg/kg) and analgesia using Tramadol (15 mg/kg). The animals were divided in three equal groups ( $n = 15$ ). Fifteen animals were implanted with Alg-Pll- $\beta$ TCP/HA composites, 15 animals were implanted with Alg-Pll-BGAuSP composites and 15 animals were implanted with Alg-Pll-BGAuIND. Of the 15 in each group, subgroups of 5 rats were humanely euthanatized at 2 weeks, 4 and 8 weeks, respectively. At the end of each experimental period, the animals were sacrificed under general anesthesia by cervical dislocation following the international standards [41].

### 2.10. Histology and immunohistochemistry assays

For histological examination, full-thickness skin samples and subcutis containing the implanted composites were collected at 14, 30 and 60 days. Each tissue was trimmed into two pieces for histological processing, fixed in 10% buffered formalin and paraffin-embedded. Serial consecutive 2–3  $\mu$ m-sections were processed for routine haematoxylin and eosin (H&E) staining. At 60 days, tissues were also evaluated by Gomori's trichrome (GT) and immunohistochemistry, using monoclonal antibody against vimentin (clone SRL33, Leica Biosystems Newcastle Ltd). For immunohistochemistry, the samples were automatically processed using Leica Bondmax™ Immunohistochemistry system (Leica Biosystems Melbourne, Bond Max model, M2 12154 series). Normal dermis in the proximity to implanted composites was used as positive control. Negative control was performed by replacing the primary antibody with normal serum from the same species. For immunohistochemistry, the positive reaction was given by the brown stain of the cytoplasm of mesenchymal cells. The average of Vimentin immunopositive cells, counted in 3 consecutive high-power fields (40 $\times$ ), was assessed for each individual at 60 days.

Additionally, liver (left lateral lobe and right medial lobe) and kidney samples were harvested for histological examination in order to evaluate the composites nanoparticles toxicity, according to Ruehl-Fehlert et al. [42] and Morawietz et al. [43]. Histological changes of the hepatic parenchyma and kidneys were graded according to the previous studies [44,45].

For both histology and immunohistochemistry, all sections were independently examined by two pathologists (M.T and C.T) using an Olympus BX41 microscope and the photomicrographs were taken using an Olympus SP350 digital camera and Stream Basic imaging software (Olympus Corporation, Tokyo, Japan). Tissue reaction induced by the implanted composites and toxic liver and renal injuries were evaluated in three serial sections for each individual (see Section 2.11).

### 2.11. Statistical analysis

All data reported in biodegradability and cell viability assay are as the mean  $\pm$  SD. The values were analysed by two-way analysis of variance ANOVA, followed by Bonferroni post-test. Statistical significance was at  $P < 0.05$  in all cases. Statistical values were obtained using GraphPad Prism 8.0 software. All measurements were repeated three times ( $n = 3$ ).

For the values of tissue reaction, which were not normally distributed, multiple pare-wise comparison was performed by one-way analysis of variance Kruskal-Wallis, followed by Dunn's Test. Spearman's correlation was the test of choice, in order to assess the correlation between non normally distributed variables. Statistical significance was at

$P < 0.05$  (95% confidence interval).

## 3. Results and discussion

### 3.1. Gold nanoparticles in bioactive glasses

For the reproducibility the sizes and shape of colloidal AuNPs and AuNPs in the glass structure were verified by UV–Vis spectroscopy (see Fig. S1 in Supplementary materials) and TEM measurements. In the glass structure were introduced the colloidal spherical gold nanoparticles (AuSP) with  $\approx 12$  nm diameter or the colloidal gold nanocages (AuIND) with  $\approx 20$  nm diameter (Fig. 2). As expected, after thermal treatments the size of AuNPs in the sample BGAuSP was around 25 nm and in the BGAuIND the gold nanocages become gold nanospheres with diameter between 11 and 25 nm (Fig. 2) [26].

The XPS measurements were performed (see Fig. 2S) to obtain the elemental composition of materials surface shown in Table 1. In both cases, the obtained results are comparable to the theoretical elemental composition, apart from gold and silver. The amount of gold is being less and the silver amount is more. The possible explanation is that Ag migrated to the surface, while Au remained below the detection depth of XPS detailed in the study by K. Magyari et al. [26].

### 3.2. Bioactive glass particles size distribution

It is known that the particle size of HA influence the inflammatory cytokine following the implantation [46]. Thus, particle size distribution of bioactive materials can affect the leukocytes response that affect regenerative signals to surrounding tissues. Dynamic light scattering (DLS) measurements was used to determine particle size distributions and the size difference between the grains that build up the BGAuSP and BGAuIND composites (Fig. 3). The size difference between glass samples is minor, the BGAuIND grains being slightly larger and the values obtained for  $\beta$ TCP/HA sample are smaller compared to the values obtained for the glass samples.

### 3.3. Structure and thermal stability of composites

FT-IR spectroscopy measurements was performed to demonstrate the cross-linking between the used materials (Fig. 4). The alginate is composed of  $\beta$ -D-mannuronic acid and  $\alpha$ -L-guluronic acid residues linked by glycosidic linkages [47,48]. Accordingly, the FT-IR spectrum contains bands given by vibrations of  $\text{COO}^-$  groups (anti-symmetric, at  $1610\text{ cm}^{-1}$ , and symmetric, at  $1418\text{ cm}^{-1}$ ), C–O–C stretching ( $1130\text{ cm}^{-1}$ ), C–C stretching ( $1092\text{ cm}^{-1}$ ) and C–O stretching ( $1022\text{ cm}^{-1}$ ) [16,47]. The structure of pullulan consists of  $\alpha$ -1,6 linked maltotriose units, which have two  $\alpha$ -1,4 glycosidic bonds [18]. Thus, the FT-IR spectrum of the pullulan present the specific vibration of these functional groups, such as CH stretching (between  $1250$  and  $1430\text{ cm}^{-1}$ ), valent vibration of C–O–C and glycosidic bridge (at  $1155\text{ cm}^{-1}$ ), stretching of C–C bond (at  $1080\text{ cm}^{-1}$ ) [20,49]. First evidence of cross-linking between alginate and pullulan is proven by the shift of anti-symmetric and symmetric stretching vibration bands of  $\text{COO}^-$  groups from  $1610$  to  $1620\text{ cm}^{-1}$  and from  $1418$  to  $1423\text{ cm}^{-1}$ , respectively (Fig. 4a) [49]. By adding the pullulan to alginate, the intermolecular hydrogen bonds originally present between the carboxylic groups are disrupted [47,49]. Since cross-linking was performed using calcium chloride, the bivalent calcium cation is strongly chelated by the OH group of pullulan and carboxyl group of alginates. The shift of C–O stretching vibration of alginate from  $1026\text{ cm}^{-1}$  to  $1031\text{ cm}^{-1}$  also indicate that the oxygen atoms from alginate create hydrogen bond with pullulan chains [49].

The used BGs in the composites are silicate glasses with typical FT-IR absorption bands: Si–O–Si asymmetric stretching ( $1050$ ,  $1230\text{ cm}^{-1}$ ), Si–O–Si bending ( $464$ ,  $800\text{ cm}^{-1}$ ) and P–O stretching ( $560\text{ cm}^{-1}$ ) [50–52]. The cross-linking between BG and polymer matrix are demonstrated by

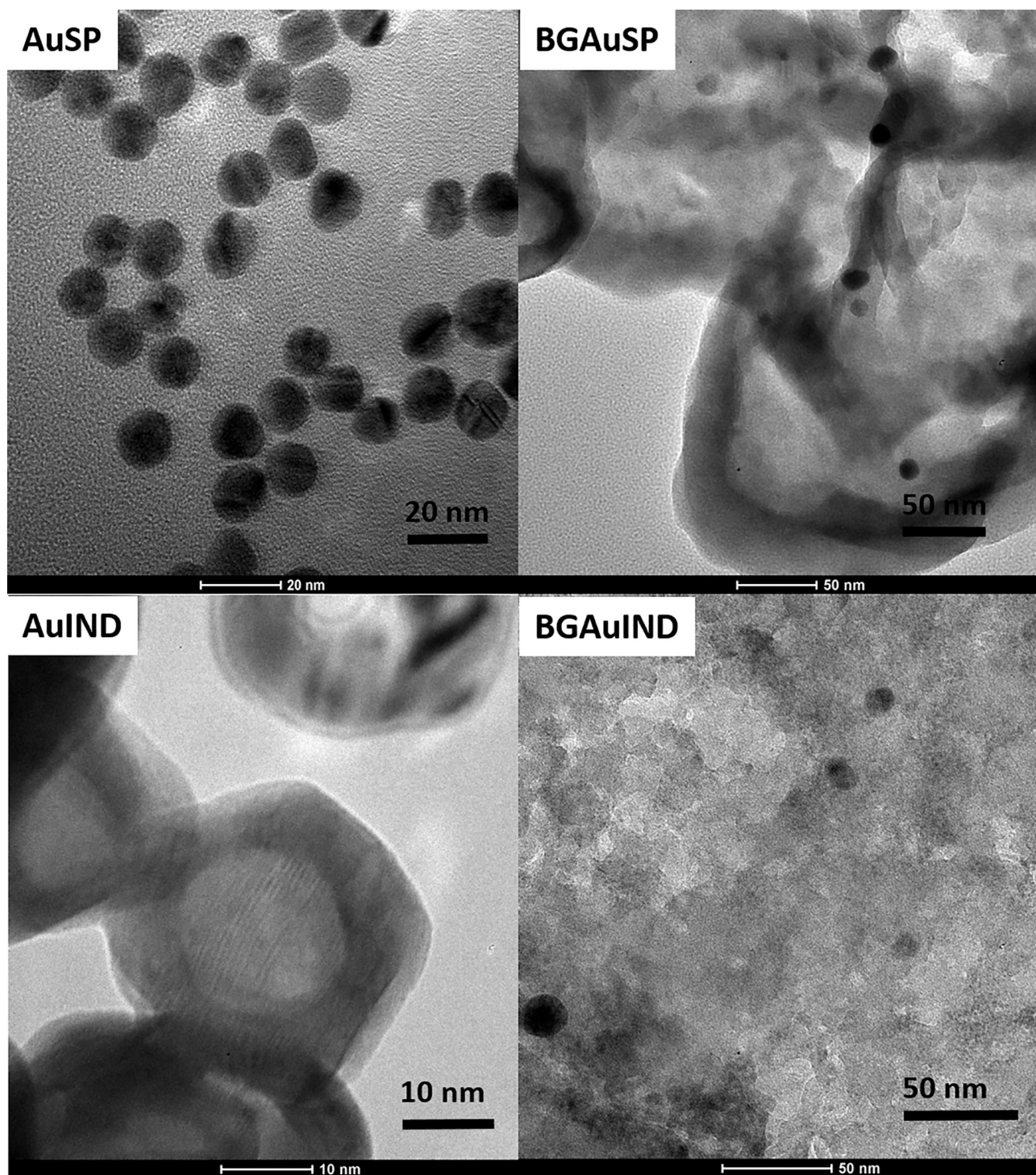


**Fig. 2.** TEM micrograph of spherical gold (AuSP), spherical gold nanocages (AuIND), bioactive glass with spherical gold (BGAuSP) and bioactive glass with spherical gold nanocages (BGAuIND). (For interpretation of the references to colour in this figure legend, the reader is referred to the web version of this article.)

additional shift of  $\text{COO}^-$  anti-symmetric stretching vibration band towards high wavelength (from  $1623$  to  $1634\text{ cm}^{-1}$ ), as a result of interaction between  $\text{COO}^-$  group from biopolymers and  $\text{Ca}^{2+}$  from BG. The shift of Si-O-Si vibration band from  $800$  to  $780\text{ cm}^{-1}$  also prove the cross-linking between used materials (Fig. 4b).

The cross-linking between  $\beta\text{TCP/HA}$  and polymer matrix was also demonstrated by the  $\text{COO}^-$  anti-symmetric stretching vibration band shift towards high wavelength (from  $1623$  to  $1634\text{ cm}^{-1}$ ) due to the interaction between  $\text{COO}^-$  group from biopolymers and  $\text{Ca}^{2+}$  from

$\beta\text{TCP/HA}$  (Fig. 4c).

The usable biomaterials must have good thermal stability concerning the process of handling before implant, for example the sterilization process. For these reasons the thermogravimetric analyses were performed (Fig. 5). From DTA thermograms, it can be seen that sodium alginate (Fig. 5a), pullulan powder (Fig. 5b) and cross-linked Alg-Pll composite (Fig. 5c) exhibit a different thermal behaviour. The behaviour of Alg-Pll and Alg-Pll-BGAuSP (Fig. 5c and d) composites are similar, indicating that the amount of glasses does not greatly influence the



**Table 1**

Elemental composition obtained from XPS measurements and calculated ones for the samples of the BGAuSP and BGAuIND.

Sample	Elemental composition (at%)						
	O	C	Ca	P	Si	Au	Ag
BGAuSP	50.3	14.7	14.2	6.2	14.5	0.1	–
BGAuSP theoretic	46.67	–	19.35	7.53	14.58	0.9	–
BGAuIND	51.3	11.4	10.2	6.8	19.7	0.03	0.57
BGAuIND theoretic	46.67	–	19.35	7.53	14.58	0.89	0.0024

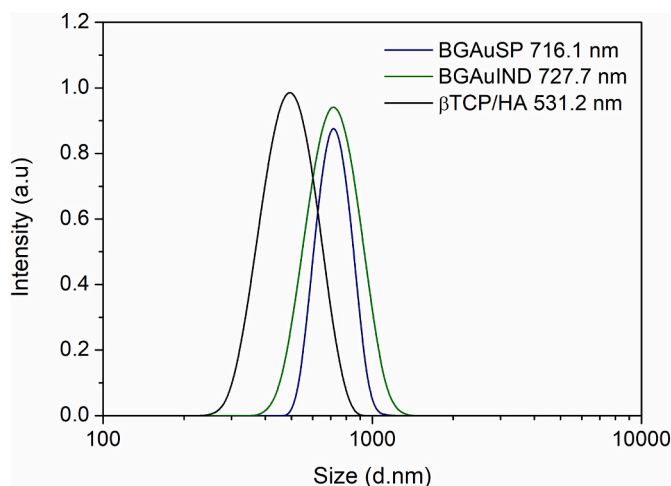


**Fig. 3.** Particle size distribution of BGAuSP (blue line), BGAuIND (green line) and  $\beta$ TCP/HA (black line) measured by DLS. (For interpretation of the references to colour in this figure legend, the reader is referred to the web version of this article.)

thermal behaviour of the material in these samples. In the temperature range between 28 and 140 °C, for all samples, occurs the dehydration, where the absorbed water molecules are eliminated. This event is evidenced by the endothermic signal with a maximum temperature around 110 °C, which corresponds to the first mass loss in the TG curves. For the sodium alginate the second exothermic signal with the maximum of 256 °C indicates the alginate decomposition by breaking the C–H bonds and breaking the bonds glycosidic C–O–C in the poly-saccharide chain, with a mass loss in TG curve of 33% (Fig. 5a) [37]. During the third degradation stage appear two exothermic signals with a maximum around 350 °C and 596 °C respectively, corresponding to the oxidation and pyrolysis process [53]. In the TG curve the degradation takes place in three steps, of approx. 46%, in total approx. 91%.

The decomposition of the polysaccharide rings in the pullulan is revealed by the exothermic signal with the maximum temperature at 294 °C (Fig. 5b) [54], followed by the oxidation of OH groups revealed by an endothermic signal with maxima at 322 °C and an exothermic signal with maxima at 452 °C respectively, which lead to the sample degradation [53]. It is noticed that in the degradation process there is a massive mass loss in two steps in a total of approx. 95%. Thus, the decomposition of the Alg and PII components is evidenced by the exothermic signal with the maximum at ~299 °C, followed by the degradation events with the exothermic signals with temperature peaks at 457 and 552 °C, respectively. Total mass loss during the degradation is of ~36%. Since the thermal events occur at higher temperatures, compared to the values obtained for Alg and PII samples, and the mass loss is considerably lower for the Alg-PII and Alg-PII-BGAuSP composites, one can infer that from a thermal point of view the sample Alg-PII-BGAuSP is more stable compare with Alg or PII.

### 3.4. Porosity and morphology analysis of composites

Materials with applications in tissue engineering must have adequate porosity. The porosity can be increased by the lyophilisation process as shown in SEM micrographs (Fig. 6), obtaining microporous materials. It can be seen that for the composites with BG the macropores range from a few micrometers up to 100  $\mu$ m, which is suitable for cell infiltration [13]. For the composite with  $\beta$ TCP/HA the macropores are much smaller, result that shows how important is the use of a suitable bioactive material as an implant.

In order to determine the porosity of the materials used, the specific surface area of both the used glasses/ceramics and the obtained composites was measured. Table 2 shows that the obtained BGs have a specific surface area of around 100 m<sup>2</sup>·g<sup>−1</sup> which indicates the presence of a microporous material. The low value for the specific surface area was obtained for commercial  $\beta$ TCP/HA, which may influence the macroporosity of the composites. The biopolymers-based composites have a small specific surface area which is specific for macroporous materials. The obtained results show the importance of the morphology of the embedded materials into the biopolymers matrix, which is an essential parameter that may affect the specific surface of the entire composites.

### 3.5. *In vitro* bioactivity and biodegradation assays of composites

It is known that *in vitro* bioactivity predict the bone regeneration ability of the materials [21,25,55]. Thus, a rapid evaluation of *in vitro* bioactivity was performed. The obtained results confirmed the appearance of an apatite layer on the materials' surface after SBF immersion (Fig. 7) as demonstrated by the following aspects:

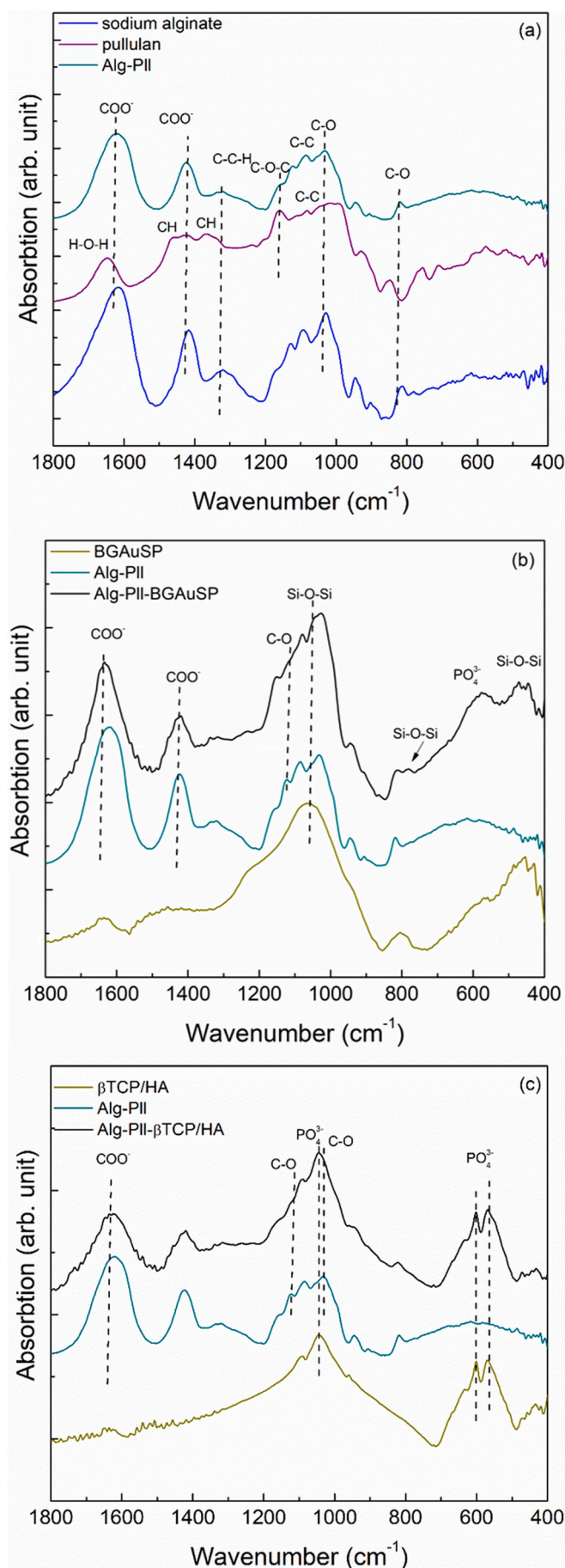
- the XRD pattern show the signature phase of HA crystalline phases at  $2\theta = 32^\circ$  and  $26^\circ$  correspond to the (112) and (002) reflection plane of a hexagonal HA crystalline structure, respectively (Fig. 7a) [56],
- the FT-IR spectra presents the specific vibration of HA at 602 and 560 cm<sup>−1</sup> associated with the bending vibration of O–P–O bonds [57] and at 1035 cm<sup>−1</sup> assigned to asymmetric stretching of P–O bonds of the phosphate group indicating the presence of self-assembled apatite layer (Fig. 7b) [50],
- SEM micrograph shows that on the materials surfaces appears a typical HA structure that is similar morphologically and in size to the HA that appeared on the BGAuSP and BGAuIND surfaces after immersion in SBF for 7 days [26]: on composite with BGAuSP surface 3D flower-like nanostructures appeared and on the composite with BGAuIND surface grain-like nanostructures were detected (Fig. 7c)

The obtained results prove the importance of choosing the best bioactive materials introduced that preserve the properties in the composite.

The determination of degradation and water absorption dynamic are very important by point of view of regeneration performance. To determine the composite weight loss and water uptake the samples was incubated in SBF. It can be seen that the biggest weight loss it takes place in first 3 days, followed by a growth due to the self-assembled apatite layer (Fig. 8a). The difference between the three samples is minor and it can be concluded that the critical period from the point of view of scaffold's performance takes place during first days.

Protein interactions and cellular adhesion on biomaterials depends on water absorption properties, considering that the body fluid transports the cell nutrients and metabolites. However, the uncontrolled swelling might have negative effects. The obtained results for the studied composites show the most reduced swelling ratio for the composite with  $\beta$ TCP/HA, but the differences from the results obtained for the other composites are minor (Fig. 8b). The relationship between the water absorption dynamic and the rate of degradation: with the apatite layer deposition increasing the absorbed water amount is also interesting finding (Fig. 8).





(caption on next column)

**Fig. 4.** FT-IR spectra of sodium alginate powder, pullulan powder and cross-linked alginate-pullulan composite (Alg-Pll) (a), BGAuSP, cross-linked Alg-Pll and Alg-Pll-BGAuSP composites (b) and βTCP/HA, cross-linked Alg-Pll and Alg-Pll-βTCP/HA composites (c).

### 3.6. *In vitro* biocompatibility of composites

Prior to studying the tissue response *in vivo*, preliminary *in vitro* studies are required, to rule out the possible toxic effect of the newly tested material [58]. In the present study, the cell type selection was based on the specific application of the biomaterial, targeting bone and wound regeneration. The viability percentage for the human fibroblast line HS 27, after 24 h, was between 85% and 103%. Interestingly, the highest viability was observed in the culture supplemented with Alg-Pll-BGAuSP composites (Fig. 9).

The viability of human osteoblasts, in the presence of all tested composites is either very close or higher than 100%, indicating no cytotoxicity in the same time frame. Moreover, the Alg-Pll-BGAuIND composites induced the proliferation of the osteoblasts with values of 113% (Fig. 9). The amount of silver content in the sample with BGAuIND does not negatively influence the fibroblast cell viability. This was to be expected, as the silver amount is 0.01% (wt) in the composite [26,36]. As for the qualitative essay, no morphological nor intra-plasmatic alterations were observed; the cells were well attached, the cytotoxicity score being 0. These results indicate cellular biocompatibility sustained by the qualitative and quantitative methods described. The actual results substantiates previous findings reported by our groups [2,24,26] regarding the BGAuSP and BGAuIND composites on human keratinocytes culture. This is also in agreement with Popescu et al. [21], who reported similar results using composites containing BG with copper oxide instead of BG with AuNPs. Notably, fibroblast and osteoblast cells viability as result of interaction with Alg-Pll composites found in our study are comparable with results obtained by Popescu et al. [21].

### 3.7. *In vivo* biocompatibility of composites

*In vivo* biomaterials compatibility was evaluated by placing subcutaneous grafts into contact with connective tissues [40]. The goal of this method is to derive preliminary information regarding the biocompatibility of biomaterials with BGAuNPs. Regarding the *in vivo* biocompatibility assay, only three composites with BGAuSP, BGAuIND and βTCP/HA were tested, since the Alg-Pll composites had been similarly tested previously [21]. The composites used in this assay are designed for future bone defect regeneration studies.

#### 3.7.1. Tissue biocompatibility

Our data reveals that the implanted scaffolds induced a mild inflammatory response and a high mesenchymal proliferative effect with formation of: a) variably sized and irregular blood channels lined by endothelial cells and b) short bundles of collagen fibers admixed with fibroblasts. No clinical implant rejection was observed by any rat (edema, swelling, discomfort), indicating a successful *in vivo* implantation of the studied composites. Several important conclusions emerged from the current study.

Initially, no gross cutaneous changes related to the implanted composites were observed in the examined samples among the three groups which is in agreement with the previous results described by Modulevsky et al. [5]. Comparable with other studies in literature, our study followed a similar timeline, ultimately demonstrating biocompatibility [59].

As for the histological evaluation, we have noticed differences between the groups. After 14 days, the Alg-Pll-βTCP/HA composite was dissolved faster than the other composites. However, the dissolution occurred towards the peripheral area in close vicinity to the fibrous capsule, muscle and cutaneous tissues (Fig. 10A). Additionally, the

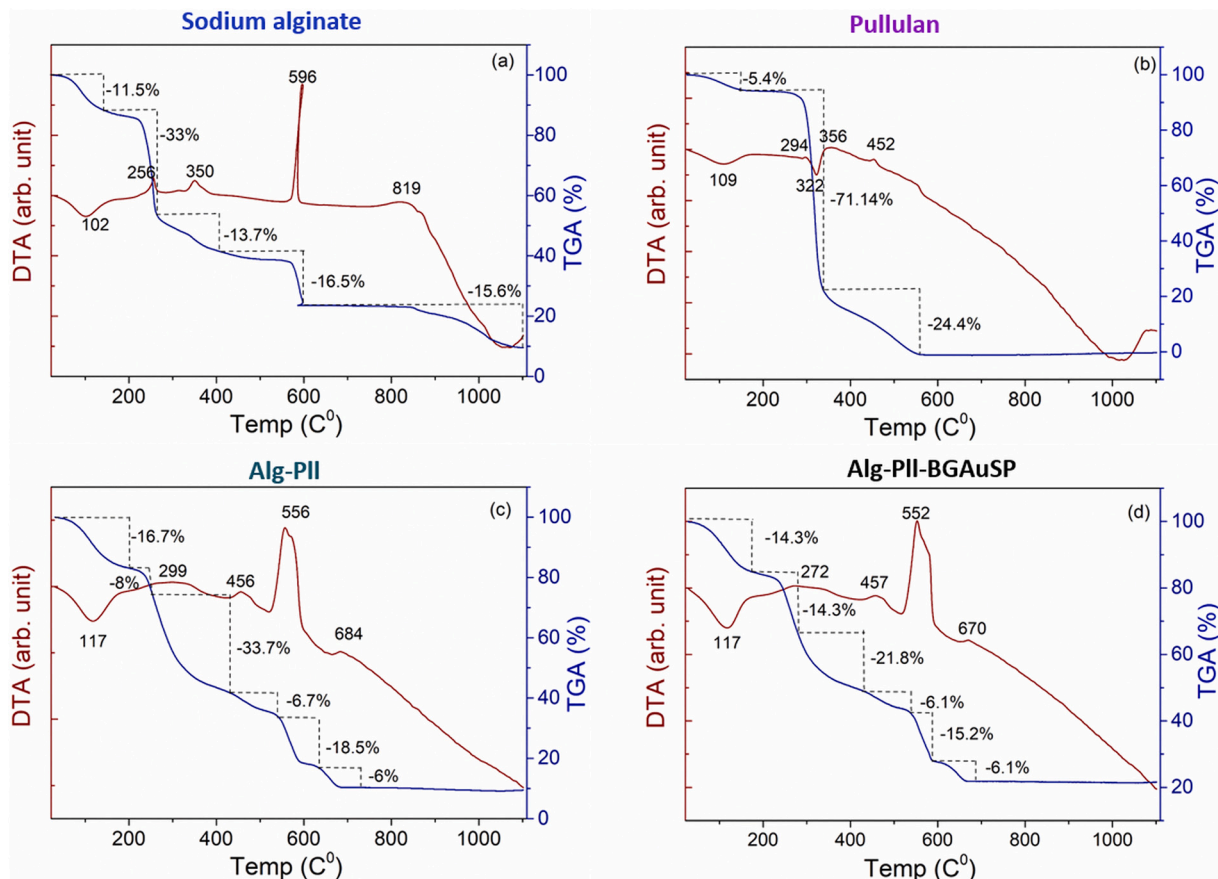


Fig. 5. DTA and TGA curves of sodium alginate (a), pullulan powder (b), cross-linked Alg-Pil (c) and Alg-Pil-BGAuSP composite (d).

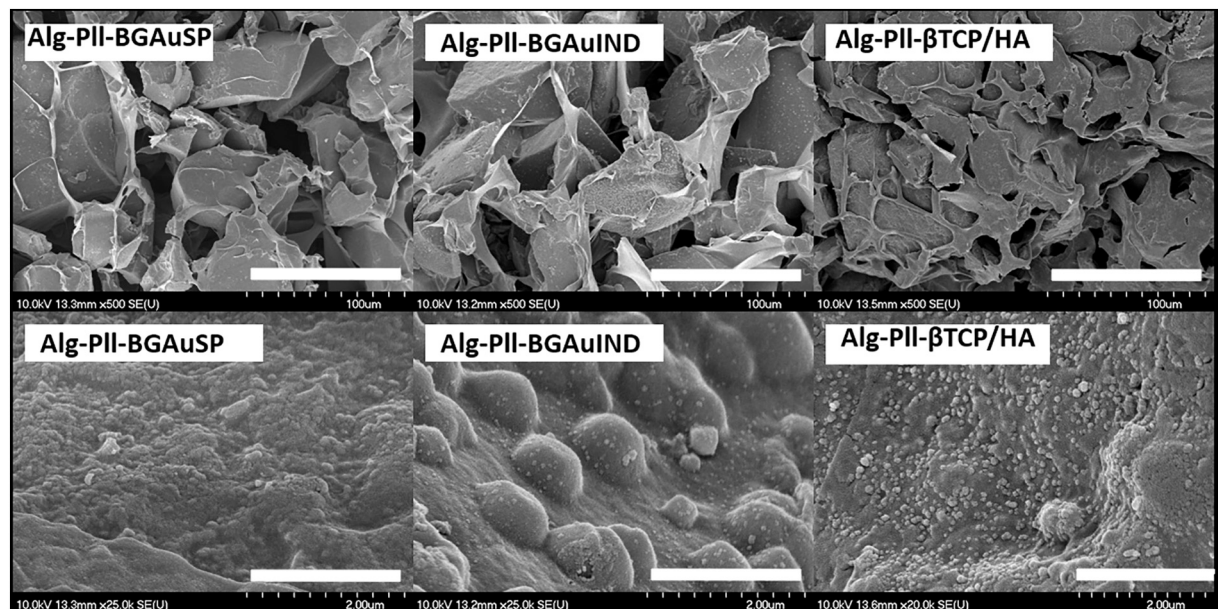


Fig. 6. SEM micrograph of Alg-Pil-BGAuSP, Alg-Pil-BGAuIND and Alg-Pil-βTCP/HA composites in different magnification. Scale bare first line 100 μm, second line 2 μm.

biomaterial released numerous geometrical, refringent crystals with a yellowish aspect (Fig. 10A1), triggering a nodular granulomatous foreign body reaction characterized by macrophages and histiocytic multinucleated giant cells (Fig. 10A1). Notably, our results are similar to those described by Massari et al. [60], where at 15 days an inflammatory

response to HA implanted subcutaneously was described.

Minor differences between the other two composites with BGAuNPs were observed microscopically. A thick layer of fibrous connective tissue encapsulated the biomaterials, but no foreign body-induced inflammatory reaction was observed (Fig. 10B–C1). During the process of the



**Table 2**

Specific surface area values of glasses/ceramics and composites.

Samples	Specific surface area ( $\text{m}^2\cdot\text{g}^{-1}$ )
BGAuSP	107
BGAuIND	87
$\beta$ TCP/HA	0.4
Alg-Pil-BGAuSP	0.6
Alg-Pil-BGAuIND	1
Alg-Pil- $\beta$ TCP/HA	0.3

biomaterial degradation and resorption, individual or small groups of active foamy macrophages created spaces within the composites with BG, which were subsequently filled by large numbers of mesenchymal cells and few collagen fibers. Formation of numerous new vascular structures filled with red blood cells was also observed, suggesting a potential angiogenic effect (Fig. 10B1, C1).

Histologically, in all groups, the composites were enclosed by a thick fibrous capsule composed of thick collagen fibers, fibroblasts and few small blood capillaries (Fig. 11A, B and C), being mildly infiltrated with small aggregates of small lymphocytes, macrophages and plasma cells. A

similar foreign body granulomatous reaction to  $\beta$ TCP/HA crystals was observed at 30 days after subcutaneous implantation of Alg-Pil- $\beta$ TCP/HA composites (Fig. 11A1). This concurs well with Massari et al. [60] and also lends support to previous findings in literature [59,61,62]. Concerning the composites with BGAuNPs (groups B and C), the processes of biomaterial degradation and resorption were more advanced compared to the group A and those described at 14 days. Thus, the channels created by foamy macrophages permeated to the centre of the biomaterial structure. These spaces were replaced by a newly formed tissue network composed of blood capillaries, supported by moderate amounts of thin collagen fibers. Small fragments of intact biomaterial were also observed at this level (Fig. 11A1, B1 and C1). Approximately, the same microscopic changes were observed with the Alg-Pil-BGAuSP and Alg-Pil-BGAuIND composites. This corresponds well with some previous findings [5] where at 4 and 8 weeks after subcutaneous implantation, new blood vessel formation within cellulose scaffolds was identified.

At 60 days post-implantation, the fibrous capsule around of implanted polymers was well developed, composed of numerous thick collagen fibers without inflammatory cells. In contrast to the materials

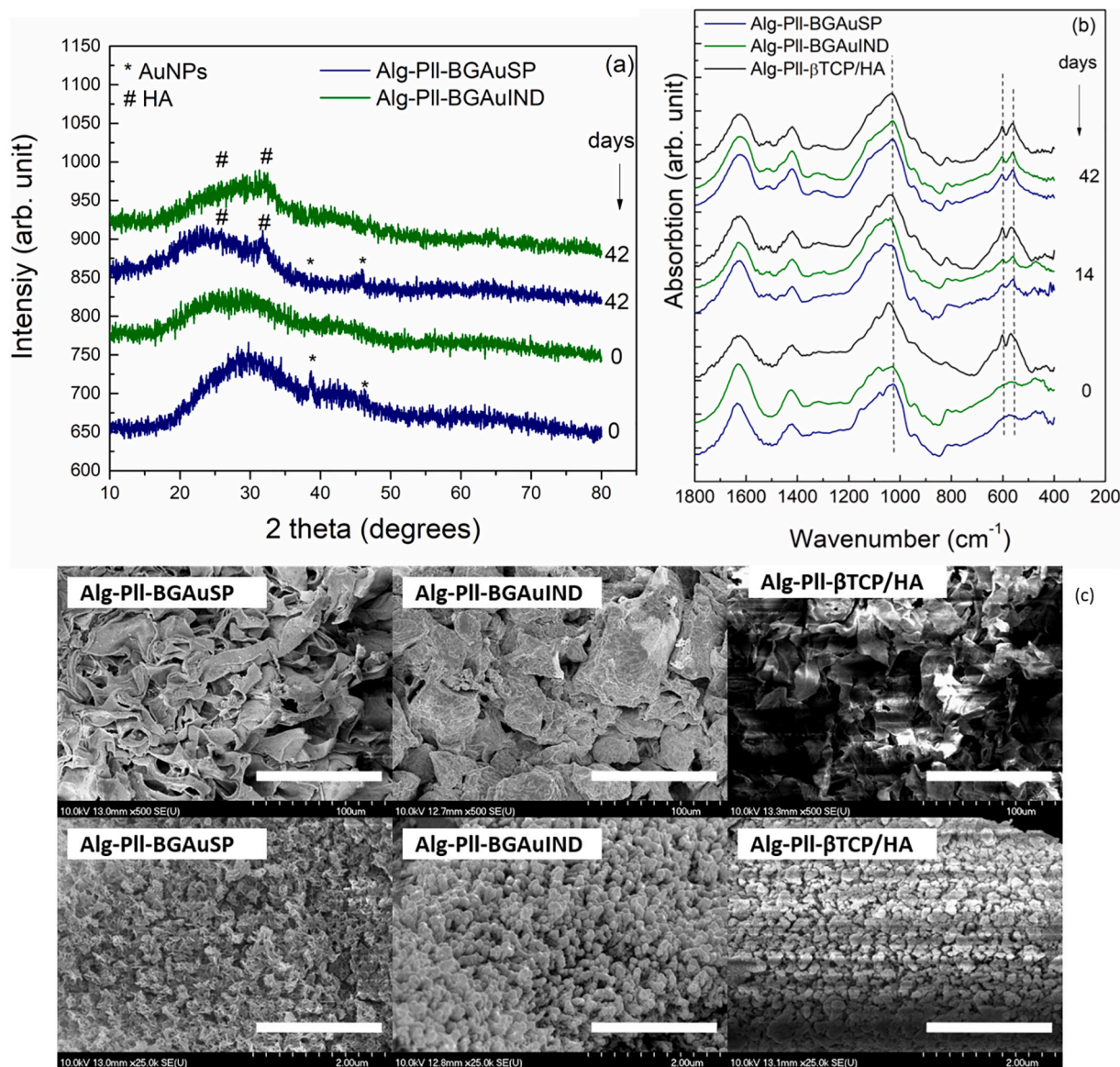


**Fig. 7.** XRD pattern (a), FT-IR spectra (b) of composites before and after immersion in SBF and SEM micrograph (c) after immersion in SBF for 42 days with different magnification Scale bare first line 100  $\mu\text{m}$ , second line 2  $\mu\text{m}$ .



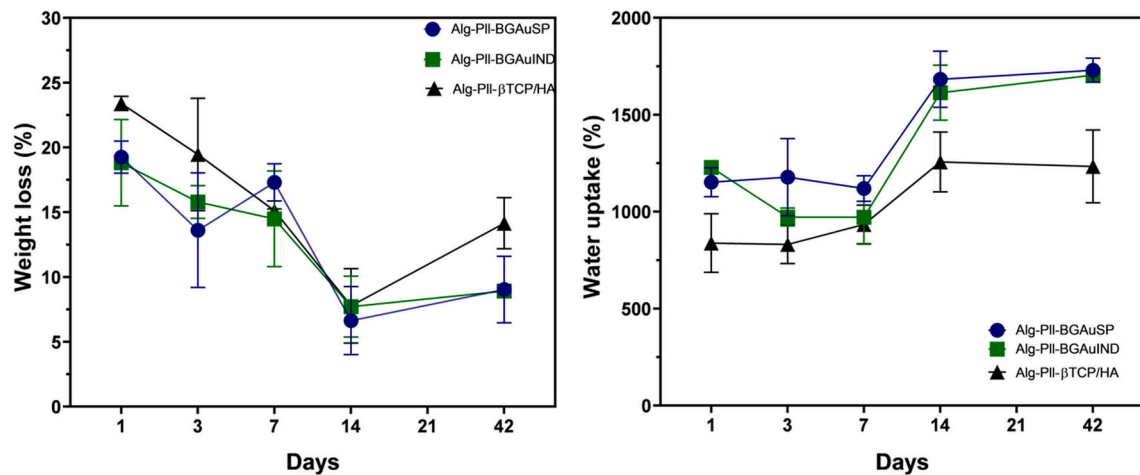


Fig. 8. Weight loss (a) and water uptake (b) of the composite scaffolds against degradation time.  $P < 0.05$ .

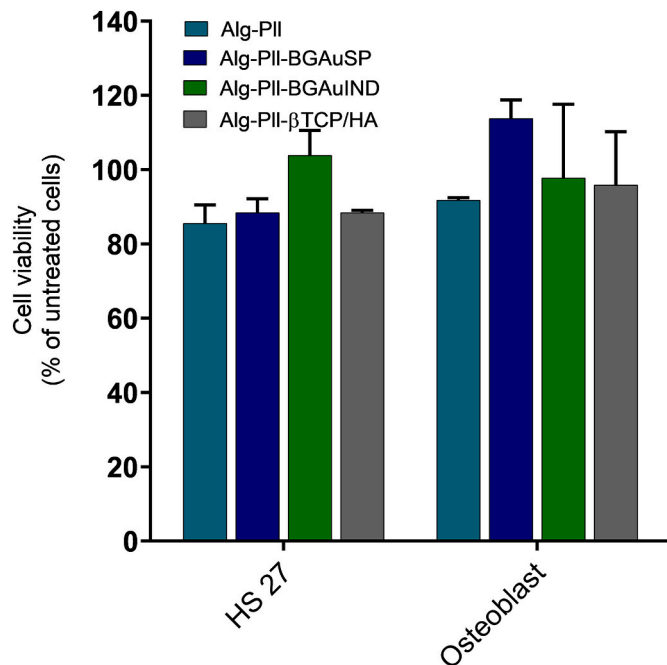


Fig. 9. Viability of HS27 and osteoblast cells after 24 h interaction with Alg-Pil, Alg-Pil-BGAuSP, Alg-Pil-BGAuIND and Alg-Pil-βTCP/HA composites at the same concentration. ( $P < 0.05$ ).

with BGAuNPs content, the connective tissue is less abundant for the composite with βTCP/HA (Fig. 12A, B and C), and a small granulomatous reaction surrounding yellow, refringent crystals of βTCP/HA was also identified (Fig. 12A1). The composite with BGAuSP showed that the fibrous tissue and the capillary network penetrated the centre part of biomaterial's structure. At the periphery of the examined area, there was marked angiogenesis and vascular spaces alongside well-defined capillaries, characterized by noticeable basophilic basal membranes and numerous endothelial cells. (Fig. 12B1). The Alg-Pil-BGAuIND showed similar aspects to the Alg-Pil-BGAuSP composite, however, the proliferated fibrous tissue was thicker and more abundant, composed of an increased number of collagen fibers, fibrocytes and blood vessels, forming a solid connective tissue network. The process of angiogenesis was marked and present across the entire surface of the material (Fig. 12C1). Small fragments of the composites were also identified into the newly formed connective tissue in all groups. As put forward by Popescu et al. [21], the evidence we found points to an absence of an

inflammatory reaction, a granulation tissue composed of proliferating fibroblasts and neovascularisation were all observed at the level of tissue-implant interphase.

This histological examination reveals that all the composites with BGAuNPs content (Alg-Pil-BGAuSP and Alg-Pil-BGAuIND) were not only well tolerated by the host's tissue, but rather induced soft tissue proliferation. This is in complete agreement with Marza et al. [24], where a strong vascular proliferation and complete wound regeneration were found by using a composite with 18%BG-AuNPs-Vaseline. The results derived from the performed investigations are correlated favourably with ours, revealing that the 18%BG-AuNPs-Vaseline ointment is a promising candidate for wound healing applications. Although our composites differ slightly it could be nevertheless argued that their purpose should be promising scaffolds in both, soft and hard tissue engineering. Furthermore, our study was successful in proving the composites tissue proliferation properties by Goldner's trichrome stain and immunohistochemical stain, by assessing collagenisation and quantitative evaluation of the newly proliferated mesenchymal cells.

### 3.7.2. Collagenization and immunoexpression of Vimentin

Collagenization was determined using Goldner's trichrome staining at 60 days following implantation. Goldner's trichrome stain showed the presence of collagen fibers in all the examined specimens. In group A (Alg-Pil-βTCP/HA), the newly formed connective tissue, within the composite showed scanty collagen fibers (Fig. 13A). Compared to the group A, the proliferated connective tissues of group B (Alg-Pil-BGAuSP) and C (Alg-Pil-BGAuIND) showed prominent deposition of the collagen bundles (Fig. 13B and C). Overall, in group C (Alg-Pil-BGAuIND) the collagenization process was more pronounced compared to group B, (Alg-Pil-BGAuSP) where the Goldner's trichrome stain revealed extensive collagen deposition, and much thicker and dense wavy collagen fibers. This is with good agreement with results provided by Modulevsky et al. [5].

Quantitative evaluation of the newly proliferated mesenchymal cells, defined as the average of positive Vimentin-stained cells/three visual high power fields (40×) (Fig. 13A1, B1, C1) confirmed the presence of a significantly higher mesenchymal cells in group C (Alg-Pil-BGAuIND;  $256.6 \pm 90.47$ ) compared with group A (Alg-Pil-βTCP/HA;  $97.8 \pm 34.79$ ) ( $P < 0.001$ ). No significant differences were found between group C (Alg-Pil-BGAuIND;  $256.6 \pm 90.47$ ) and group B (Alg-Pil-BGAuSP;  $184.6 \pm 49.74$ ), thus the silver content in the Alg-Pil-BGAuIND sample has no negative effect. ( $P > 0.5$ ). However, we cannot say with certainty that silver is responsible for this soft tissue result in group C (Alg-Pil-BGAuIND).

Currently there is an interest in developing bioactive and biocompatible biomaterials which will degrade *in vivo* and act as a temporary



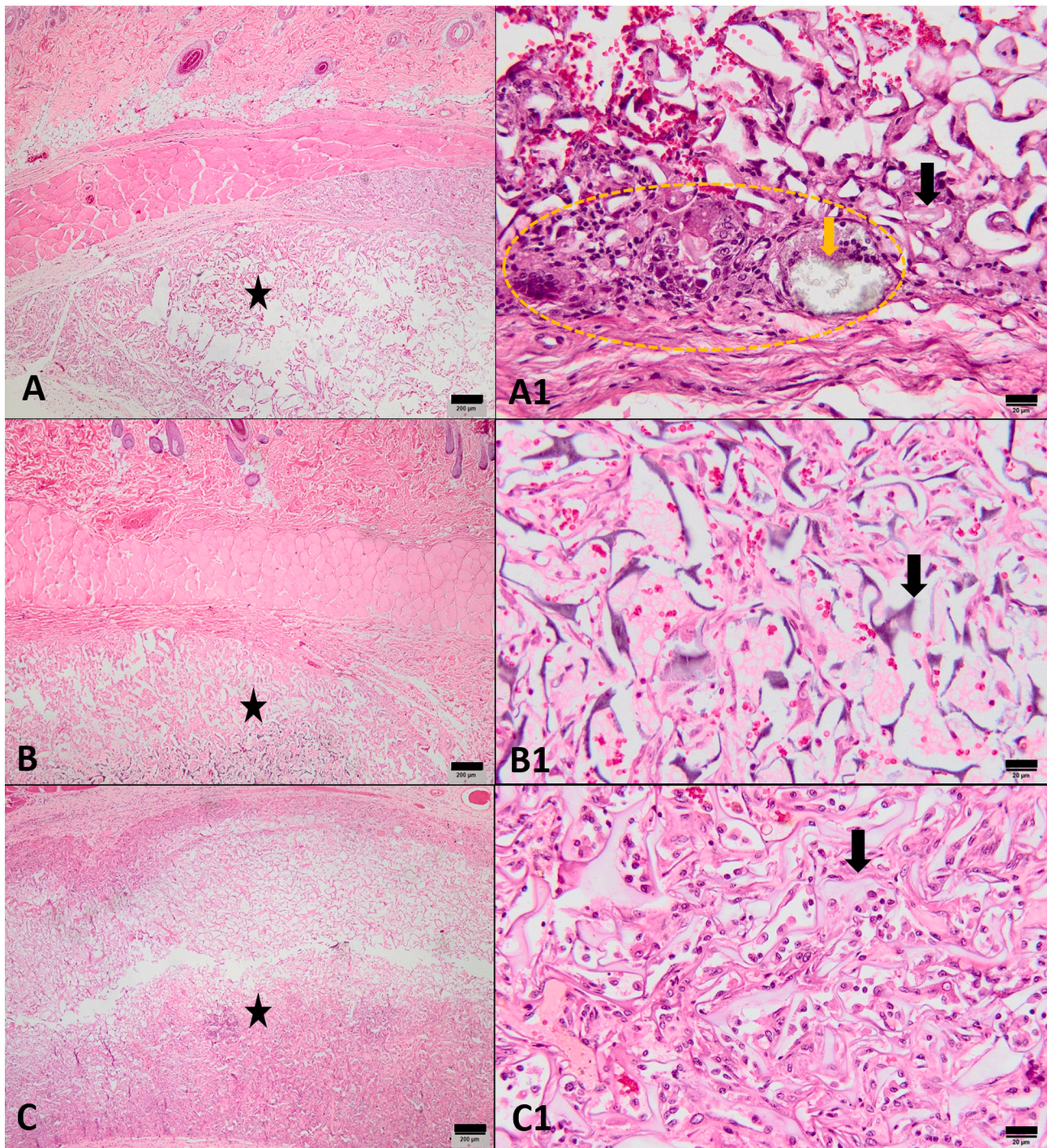


**Fig. 10.** Histomorphology of the local response induced by implanted composites in rat subcutaneous tissues at 14 days. Group A (A, A1) represents the Alg-Pil- $\beta$ TCP/HA composites; Group B (B, B1) represents Alg-Pil-BGAuSP composites; Group C (C, C1) represents Alg-Pil-BGAuIND composites. Note the fragments of biodegradable scaffold (black stars) in proximity to the fibrous capsule, muscle and cutaneous tissue (A, B and C). Fig. A1 showing a cluster of lymphocytes, macrophages and histiocytic multinucleated giant cells (encircled area) surrounding numerous pale yellow refringent crystals (orange arrow). The biomaterial (black arrows) was degraded by macrophages, invaded and partially replaced by numerous mesenchymal cells, consisting of fibroblasts and endothelial cells, occasionally forming new blood tunnels filled with red blood cells (A1, B1, C1). H&E staining. Scale bars: A–C = 200  $\mu$ m, A1–C1 = 20  $\mu$ m. (For interpretation of the references to colour in this figure legend, the reader is referred to the web version of this article.)

scaffold with the potential to promote and support the regeneration of damaged tissue. Our scaffolds demonstrated pro-angiogenesis qualities which are critical for blood transport for the surrounded tissue. Interestingly, the time frame of an 8 weeks periods also appeared in various other studies [63,64]. This is an ideal scenario, where newly formed structures are found while the scaffolds degrade. Additionally,

noteworthy correlation exists between the results found *in vivo* and *in vitro*, based on the same composites. It seems the Alg-Pil-BGAuIND has the most proliferative effect on fibroblasts cultural cells and also in the subcutaneous tissue, suggesting a new biomaterial for tissue regeneration.



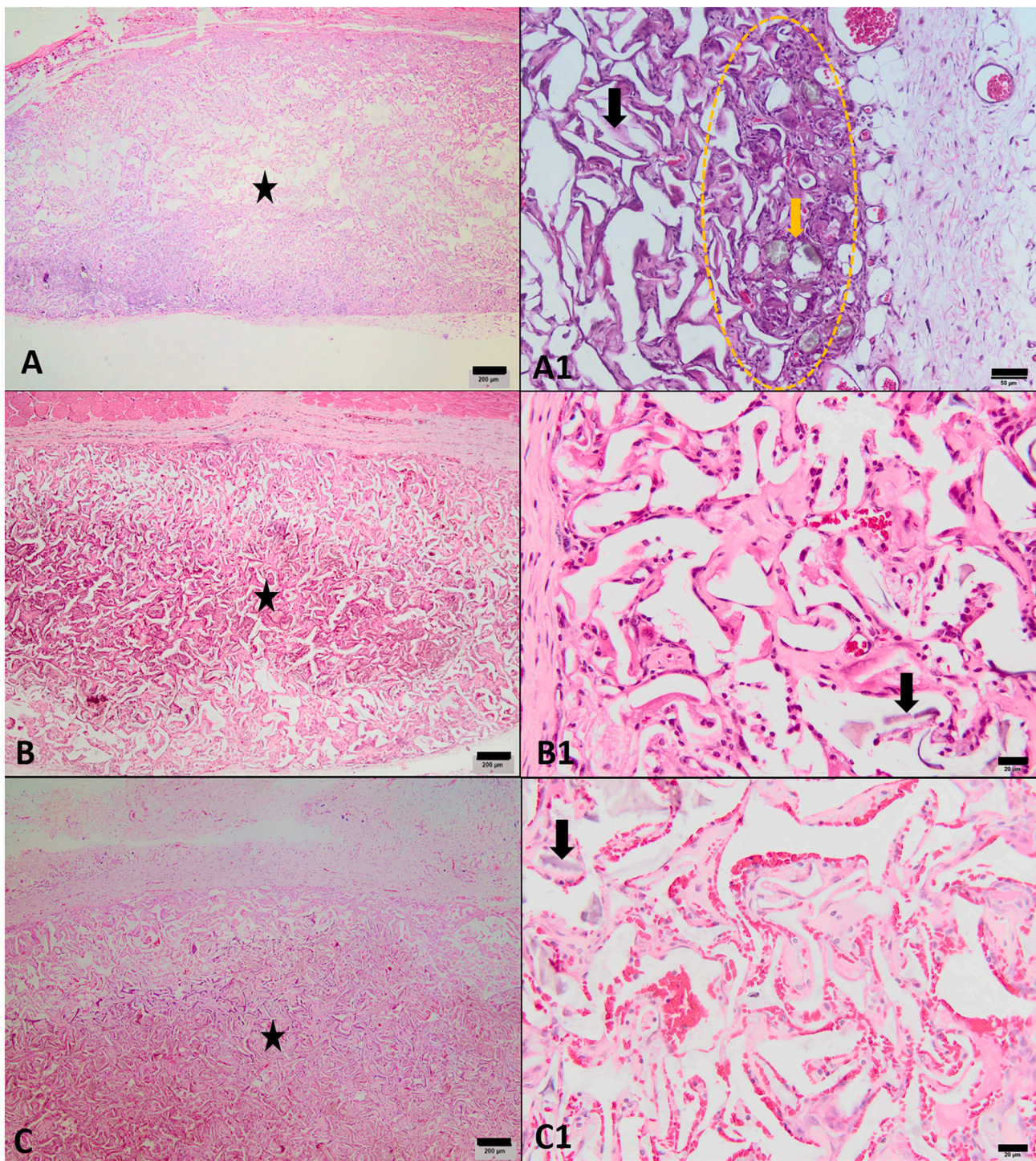


**Fig. 11.** Histomorphology of the local response induced by implanted composites in rat subcutaneous tissues at 30 days. Group A (A, A1) represents the Alg-Pll- $\beta$ TCP/HA composites; Group B (B, B1) represents Alg-Pll-BGAuSP composites; Group C (C, C1) represents Alg-Pll-BGAuIND composites. Note the fragments of biodegradable scaffold (black stars) in the center of the implanted areas (A, B and C). Fig. A1 revealing a group of lymphocytes, macrophages and histiocytic multinucleated giant cells (encircled area) delimiting pale yellow refringent crystals (orange arrow). Small fragments of degraded biomaterial (black arrows) is retained into a newly formed connective tissue network composed of numerous mesenchymal cells, occasionally forming new blood channels and supported by moderate amounts of collagen fibers (A1, B1 and C1). H&E staining. Scale bars: A–C = 200  $\mu$ m, A1–C1 = 20  $\mu$ m. (For interpretation of the references to colour in this figure legend, the reader is referred to the web version of this article.)

### 3.7.3. Organ toxicity

AuNPs are actively being used for diagnostics and therapeutic purposes. They are commonly used in cancer therapy as a delivery vector of chemical substances in solid tumours. In experimental studies, no accumulation in the liver, spleen or other healthy organ was identified;

however, such AuNPs were identified in the tumoral cells [65,66]. A pertinent question with regards to biodistribution, blood stream circulation and pharmacokinetics was then raised. Due to discrepancies in data concerning toxicity estimations in various experimental designs, a simple way to streamline results obtained from future studies is to



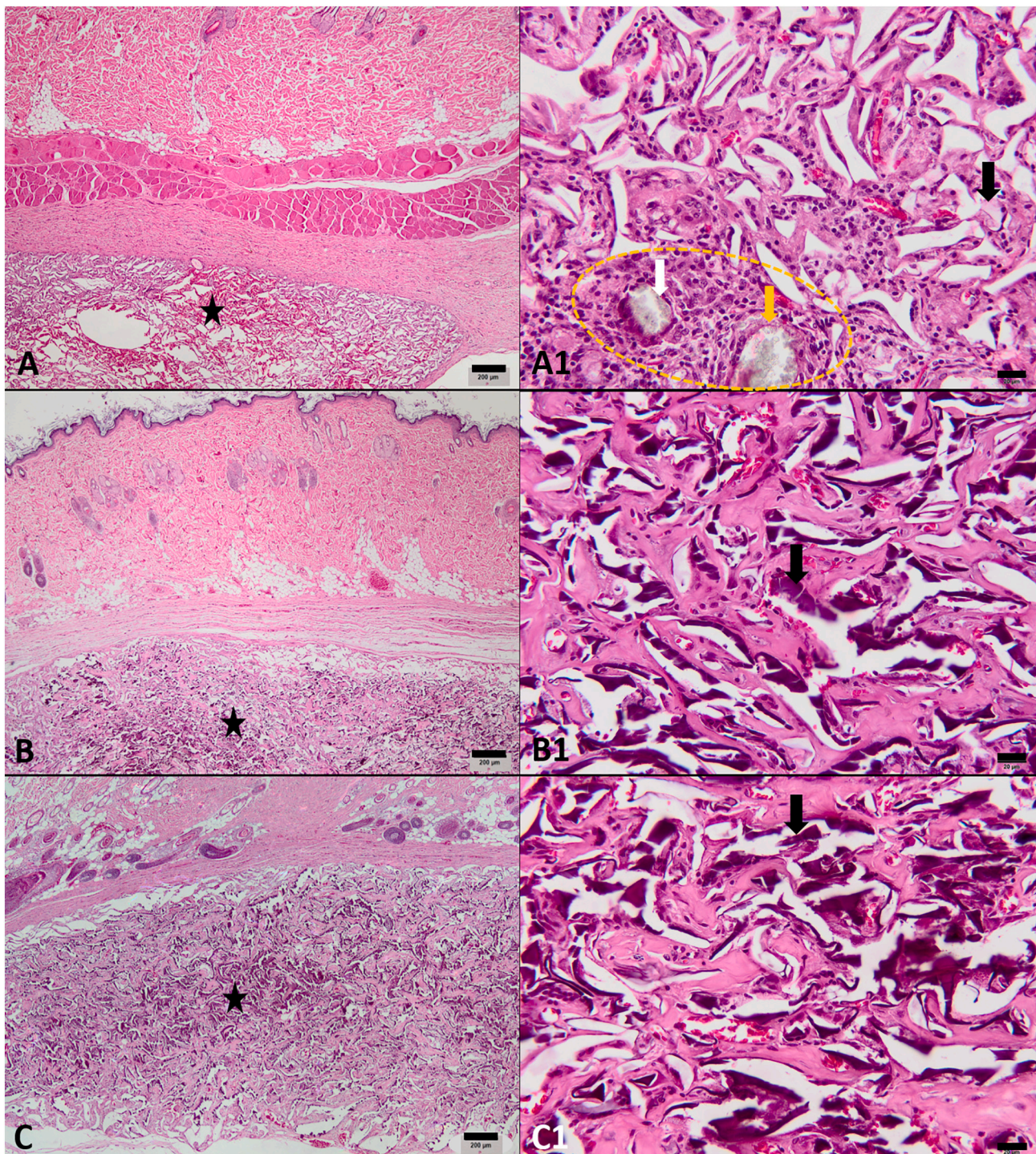


**Fig. 12.** Histological features of the local response induced by implanted composites in rat subcutaneous tissues at 60 days. Group A (A, A1) represents the Alg-Pll- $\beta$ TCP/HA composites; Group B (B, B1) represents the Alg-Pll-BGAuSP composites; Group C (C, C1) represents Alg-Pll-BGAuIND composites. The subcutis is expanded by implanted composites (black stars) enclosed by a dense fibrous capsule (A, B and C). The entire surface of the implanted composites is penetrated by newly formed blood capillaries supported by thick eosinophilic collagen fibers. Small fragments of composites (black arrows) are embedded into the connective tissue (black arrows) (A1, B1 and C1). A small granulomatous reaction (A1, delimited area) surrounding yellow refringent crystals of HA (orange arrow) was identified only in the group A. H&E staining. Scale bars: A–C = 200  $\mu$ m, A1–C1 = 20  $\mu$ m. (For interpretation of the references to colour in this figure legend, the reader is referred to the web version of this article.)

perform a toxicity study, whether it is systemic or targeted to a specific organ. Whereas the *in vitro* studies demonstrate conclusions relating to the size, shape and functionalization methods of biomaterials with AuNPs, the *in vivo* data, is rather scarce and inconsistent [9]. Nevertheless, smaller nanoparticles of 1–2 nm in diameter are believed to be

more toxic since a possibility of irreversible binding to biopolymers and biological proteins in the cells and blood exist [9]. In our study, subacute organ toxicity at both 14 and 30 days was evaluated in order to test whether or not the studied biomaterials with AuNPs with diameter between 11 and 25 nm [26] prove to be toxic for the system; our goal was



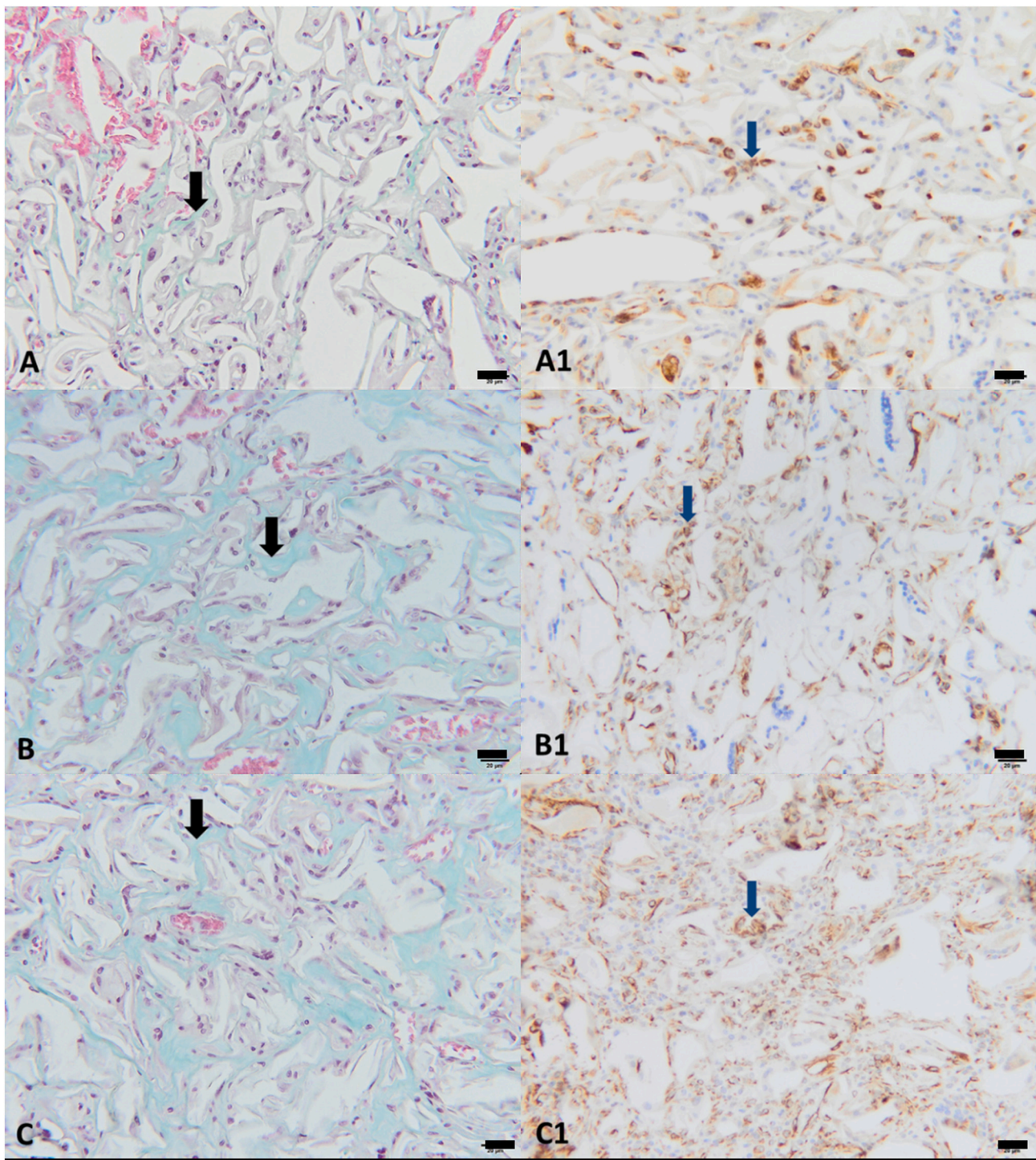


**Fig. 13.** Morphological features of collagenization and Vimentin immunoeexpression in the proliferated connective tissue within subcutaneous implanted composites. A–C) Goldner's trichrome stained specimens showing a variable intensity collagen deposition (black arrows) in group A (Alg-Pil- $\beta$ TCP/HA), group B (Alg-Pil-BGAuSP) and group C (Alg-Pil-BGAuIND). A1–C1). Immunohistochemical staining for Vimentin revealing variable numbers of newly proliferated mesenchymal cells (blue arrows) in group A (A1), group B (B1) and group C (C1), IHC stain, haematoxylin counterstain. Scale bars: A–C, A1–C1 = 20  $\mu$ m. (For interpretation of the references to colour in this figure legend, the reader is referred to the web version of this article.)

to test whether the nanoparticles themselves, encased in the biomaterial, were safe. Both the liver and kidneys presented, in all groups, normal histological features (Fig. 14). In a small number of individuals, a mild renal and hepatic congestion was observed; however, this may be attributed to the euthanasia protocol. It can be deduced that the studied composites lack organ toxicity and are biocompatible. Even though these results differ from some earlier studies, which stated that

intermediate size nanoparticles, 18–37 nm, were linked to organ damage (liver, spleen, lungs) [67] they are consistent with those of Kattumuri et al. [68], where the NPs accumulated in lung and liver, no side effects were observed. This is consistent with results obtained by Xing et al. [69], where cellulose hydrogels containing black phosphorus nanoparticles were injected subcutaneously in mice. After two weeks, no modifications in body weight and no histological modifications in the



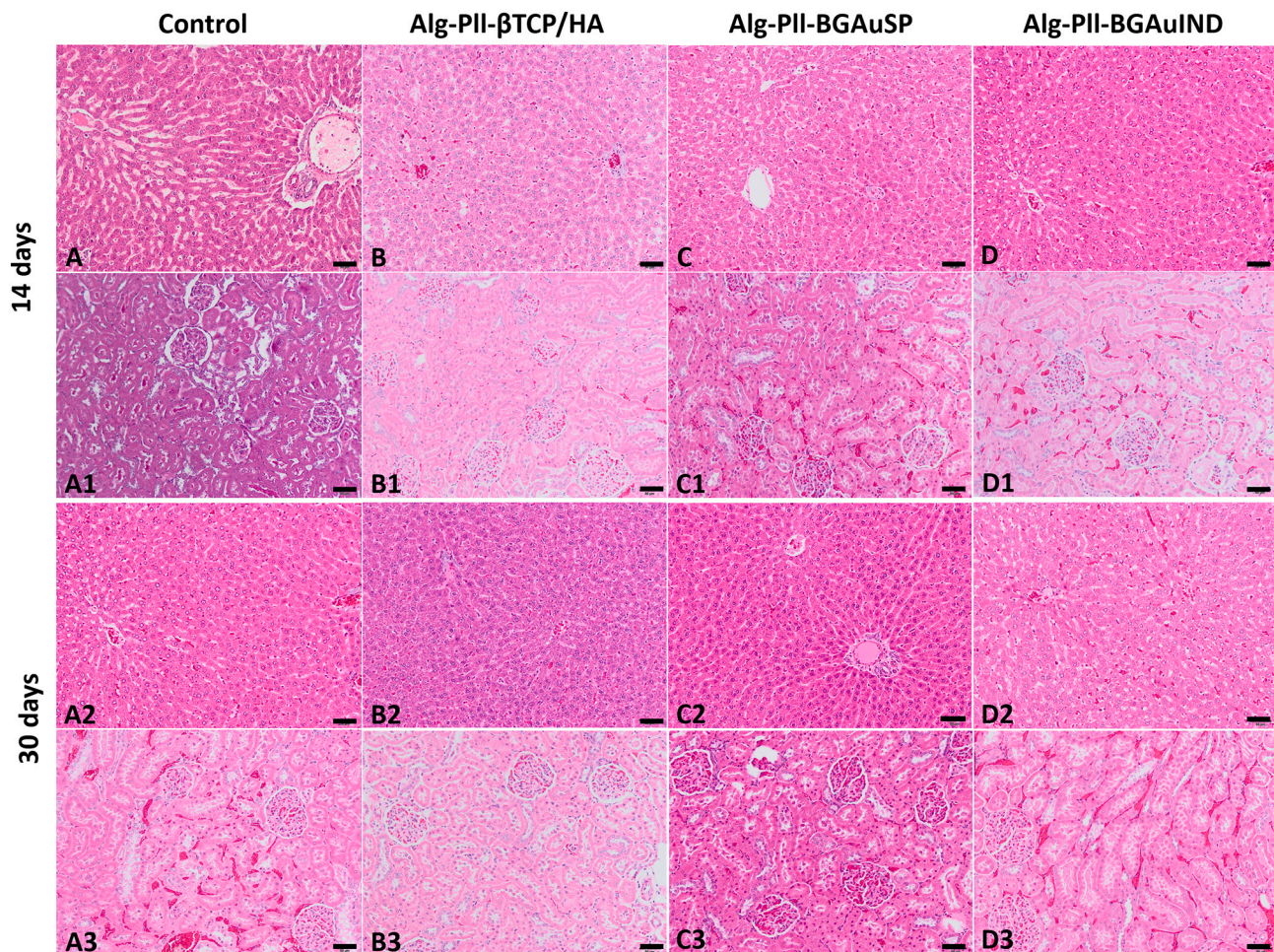


**Fig. 14.** Histological findings of liver and kidney after 14 and 30 days studied biomaterial implantation. No significant histological changes were identified in all examined groups. Group A (A–A3) represents the control; Group B (B–B3) is the Alg-Pll- $\beta$ TCP/HA composites; Group C (C–C3) represents Alg-Pll-BGAuSP composites; Group D (D–D3) is Alg-Pll-BGAuIND composites. H&E staining. Scale bars: A–D3 = 50  $\mu$ m.

major organs (heart, liver, spleen, lung and kidney) were observed. This is in good agreement with toxicokinetic studies where kidney damages were not noticed, even though a size dependent biodistribution could be highlighted. An interesting question regarding the bioparticles elimination route should be considered due to the resistance to renal excretion [70–72]. It is fundamental to note that the amount of silver in the Alg-Pll-BGAuIND composite is insignificant (0.01% (wt) in the composite), and therefore organ toxicity is excluded but it could rather have an antimicrobial effect as suggested by Magyari et al. [26].

The biocompatibility results obtained on Alg-Pll-BGAuSP and Alg-Pll-BGAuIND composites show promising clinical applications in orthopedics, both in veterinary and human medicine. It can be used as a graft in bone defects and in various surgical procedures in the idea that it could enhance bone healing and osteogenesis. For example, it can be of use in the Tibial Tuberosity Advancement (TTA) surgical procedure [73,74] which is a new and alternative method used to treat cranial cruciate ligament disease and these biomaterials should be capable of inducing enhanced bone regeneration and prevent post-operative complications.

#### 4. Conclusions

Biopolymer-bioactive glass composites with AuNPs were successfully synthesized, characterized, and investigated *in vitro* and *in vivo*. The FT-IR spectra revealed the cross-linking between polymers and glass-ceramics and the DTA and TGA curves demonstrated a suitable

thermal stability for sterilization process. The *in vitro* assays demonstrated adequate form and behaviour: the pore size of composites ranged from a few micrometers up to 100, which is suitable for cell infiltration, the self-assembled apatite layer after SBF immersion confirmed the bioactivity. The degradation rate is critical in the first three days, after which the self-assembled apatite layer stabilized the degradation.

Viability assays have highlighted optimal cellular proliferation and *in vitro* biocompatibility. It is important to note that Alg-Pll-BGAuSP composites had a greater effect on osteoblasts while Alg-Pll-BGAuIND composites had a better effect on fibroblasts. Despite these results, the cause of these effects remains unclear. Our study has led us to conclude, based on the *in vivo* subcutaneous analysis that the composites based on Alg-Pll-BGAuNP have shown excellent biocompatibility at 14, 30 and 60 days, showing marked angiogenesis and tissue proliferation in comparison to the Alg-Pll- $\beta$ TCP/HA composite, which provoked an immune response represented by a foreign body reaction. Based on the histopathological results obtained at 60 days, we observed a potential soft tissue regeneration which led us to perform an immunohistochemical analysis, which succeeded in demonstrating an intense collagenization process and mesenchymal cell differentiation with the Alg-Pll-BGAuNP composites. Furthermore, with the same biomaterials, we have also managed to demonstrate a lack of organ toxicity.

Our research paper underlined another noteworthy correlation that exists between the results found *in vivo* and *in vitro*, based on the same composites. It seems the Alg-Pll-BGAuIND has the most proliferative effect on fibroblasts cultural cells and also in the subcutaneous tissue,



suggesting a new biomaterial for soft tissue regeneration. Taken together these results suggest promising, innovative, and biocompatible composites with bioactive properties for future soft tissue and bone engineering endeavours.

### CRedit authorship contribution statement

The manuscript was written through contributions of all authors. All authors have given approval to the final version of the manuscript.

Nr. Crt.	Author	Contribution
1	Dreanca, Alexandra	Conceptualization, Investigation, Methodology, Visualization, Roles/Writing – original draft, Writing – review & editing
2	Marieta Muresan-Pop	Formal analysis, Investigation, Roles/Writing – original draft
3	Marian Taulescu	Investigation, Methodology, Supervision, Roles/Writing – original draft, Writing – review & editing
4	Zsejke-Réka Tóth	Formal analysis, Investigation, Visualization, Roles/Writing – original draft
5	Bogdan, Sidonia	Investigation, Methodology
6	Cosmin Pestean	Investigation, Methodology
7	Stephie Oren	Investigation
8	Corina Toma	Investigation
9	Andra Popescu	Investigation
10	Emőke Páll	Investigation, Methodology
11	Sevastre, Bogdan	Validation, Roles/Writing – original draft
12	Baia, Lucian	Validation, Roles/Writing – original draft
13	Magyari, Klára	Conceptualization, Formal analysis, Funding acquisition, Methodology, Project administration, Supervision, Visualization, Roles/Writing – original draft, Writing – review & editing

### Declaration of competing interest

The authors declare that they have no known competing financial interests or personal relationships that could have appeared to influence the work reported in this paper.

### Acknowledgement

This work was supported by a grant of Ministry of Research and Innovation, CNCS - UEFISCDI, project number PN-III-P1-1.1-TE-2016-1324, within PNCID III. K. Magyari acknowledges the support of the János Bolyai Research Scholarship of the Hungarian Academy of Sciences BO/00066/19/7 and MTA Domus 3031/28/2019/HTMT. Authors would like to thank Kecsenovity Egon for carrying out the TEM measurements.

### Appendix A. Supplementary data

Supplementary data to this article can be found online at <https://doi.org/10.1016/j.msec.2021.112006>.

### References

- [1] A.M. Craciun, M. Focsan, K. Magyari, A. Vulpoi, Z. Pap, Surface plasmon resonance or biocompatibility-key properties for determining the applicability of noble metal nanoparticles, *Materials* (Basel). 10 (2017) 836–873, <https://doi.org/10.3390/ma10070836>.
- [2] K. Magyari, T. Nagy-Simon, A. Vulpoi, R.A. Popescu, E. Licarete, R. Stefan, K. Hernádi, I. Papuc, L. Baia, Novel bioactive glass-AuNP composites for biomedical applications, *Mater. Sci. Eng. C*. 76 (2017) 752–759, <https://doi.org/10.1016/j.msec.2017.03.138>.
- [3] A. Bonici, G. Lusvardi, G. Malavasi, L. Menabue, A. Piva, Synthesis and characterization of bioactive glasses functionalized with Cu nanoparticles and organic molecules, *J. Eur. Ceram. Soc.* 32 (2012) 2777–2783, <https://doi.org/10.1016/j.jeurceramsoc.2012.02.058>.
- [4] S. Ferraris, M. Miola, A. Cochis, B. Azzimonti, L. Rimondini, E. Prenesti, E. Vernè, In situ reduction of antibacterial silver ions to metallic silver nanoparticles on bioactive glasses functionalized with polyphenols, *Appl. Surf. Sci.* 396 (2017) 461–470, <https://doi.org/10.1016/j.apsusc.2016.10.177>.
- [5] D.J. Modulevsky, C.M. Cuierrier, A.E. Pelling, Biocompatibility of subcutaneously implanted plant-derived cellulose biomaterials, *PLoS One* 11 (2016) 1–19, <https://doi.org/10.1371/journal.pone.0157894>.
- [6] M. Saini, Implant biomaterials: a comprehensive review, *World J. Clin. Cases* 3 (2015) 52, <https://doi.org/10.12998/wjcc.v3.i1.52>.
- [7] E.T. Pashuck, M.M. Stevens, Designing regenerative biomedical therapies for the clinic, *Biomater.* 4 (160) (2012) 1–12, <https://doi.org/10.1126/scitranslmed.3002717>.
- [8] M. Fathi-Achachelouei, H. Knopf-Marques, C.E. Ribeiro da Silva, J. Barthès, E. Bat, A. Tezcaner, N.E. Vrana, Use of nanoparticles in tissue engineering and regenerative medicine, *Front. Bioeng. Biotechnol.* 7 (2019) 1–22, <https://doi.org/10.3389/fbioe.2019.00113>.
- [9] L.A. Dykman, N.G. Khlebtsov, *Gold Nanoparticles in Biology and Medicine: Recent Advances and Prospects* 3, 2011, pp. 34–55.
- [10] M. Adabi, M. Naghibzadeh, M. Adabi, M.A. Zarrinfard, S.S. Esnaashari, A. M. Seifalian, R. Faridi-Majidi, H. Tanimowo Aiyelabegan, H. Ghanbari, Biocompatibility and nanostructured materials: applications in nanomedicine, *Artif. Cells Nanomed. Biotechnol.* 45 (2017) 833–842, <https://doi.org/10.1080/21691401.2016.1178134>.
- [11] C.J. Kirkpatrick, Modelling the regenerative niche: a major challenge in biomaterials research, *Regen. Biomater.* 2 (2015) 267–272, <https://doi.org/10.1093/rb/rbv018>.
- [12] A. Kashirina, Y. Yao, Y. Liu, J. Leng, Biopolymers as bone substitutes: a review, *Biomater. Sci.* 7 (2019) 3961–3983, <https://doi.org/10.1039/c9bm00664h>.
- [13] J. Venkatesan, I. Bhatnagar, P. Manivasagan, K.H. Kang, S.K. Kim, Alginate composites for bone tissue engineering: a review, *Int. J. Biol. Macromol.* 72 (2015) 269–281, <https://doi.org/10.1016/j.ijbiomac.2014.07.008>.
- [14] M.R. Rekha, C.P. Sharma, Pullulan as a promising biomaterial for biomedical applications: a perspective, *Trends Biomater. Artif. Organs* 20 (2007) 111–116.
- [15] S.J. Bidarra, C.C. Barrias, P.L. Granja, Injectable alginate hydrogels for cell delivery in tissue engineering, *Acta Biomater.* 10 (2014) 1646–1662, <https://doi.org/10.1016/j.actbio.2013.12.006>.
- [16] P. Prasad, G.S. Guru, H.R. Shivakumar, K. Sheshappa Rai, Investigation on miscibility of sodium alginate/pullulan blends, *J. Polym. Environ.* 20 (2012) 887–893, <https://doi.org/10.1007/s10924-012-0427-4>.
- [17] V.W. Wong, K.C. Rustand, M.G. Galvez, E. Neofytou, J.P. Glotzbach, M. Januszky, M.R. Major, M. Sorkin, M.T. Longaker, J. Rajadas, D. Ph, G.C. Gurtner, Engineered pullulan-collagen composite dermal hydrogels improve early cutaneous wound healing, *Tissue Eng. A* 17 (5–6) (2011) 631–644, <https://doi.org/10.1089/ten.tea.2010.0298>.
- [18] R.S. Singh, N. Kaur, V. Rana, J.F. Kennedy, Recent insights on applications of pullulan in tissue engineering, *Carbohydr. Polym.* 153 (2016) 455–462, <https://doi.org/10.1016/j.carbpol.2016.07.118>.
- [19] K.C. Cheng, A. Demirci, J.M. Catchmark, Pullulan: biosynthesis, production, and applications, *Appl. Microbiol. Biotechnol.* 92 (2011) 29–44, <https://doi.org/10.1007/s00253-011-3477-y>.
- [20] Y. Sakata, M. Otsuka, Evaluation of relationship between molecular behaviour and mechanical strength of pullulan films, *Int. J. Pharm.* 374 (2009) 33–38, <https://doi.org/10.1016/j.ijpharm.2009.02.019>.
- [21] R.A. Popescu, K. Magyari, M. Taulescu, A. Vulpoi, C. Berce, S. Bogdan, C. Lelescu, A. Dreanca, O. Tudoran, I. Papuc, L. Baia, New alginate–pullulan–bioactive glass composites with copper oxide for bone tissue regeneration trials, *J. Tissue Eng. Regen. Med.* 12 (2018) 2112–2121, <https://doi.org/10.1002/term.2746>.
- [22] R.A. Popescu, F.A. Tăbăran, S. Bogdan, A. Fărcășanu, R. Purdoi, K. Magyari, A. Vulpoi, A. Dreanca, B. Sevestre, S. Simon, I. Papuc, L. Baia, Bone regeneration response in an experimental long bone defect orthotopically implanted with alginate–pullulan–glass–ceramic composite scaffolds, *J. Biomed Mater Res B Appl Biomater* 108 (2020) 1129–1140, <https://doi.org/10.1002/jbm.b.34464>.
- [23] A.R. Boccaccini, M. Erol, W.J. Stark, D. Mohn, Z. Hong, J.F. Mano, Polymer/bioactive glass nanocomposites for biomedical applications: a review, *Compos. Sci. Technol.* 70 (2010) 1764–1776, <https://doi.org/10.1016/j.compscitech.2010.06.002>.
- [24] S.M. Mărza, K. Magyari, S. Bogdan, M. Moldovan, C. Peștean, A. Nagy, F. Tăbăran, E. Licarete, S. Suarasan, A. Dreanca, L. Baia, I. Papuc, Skin wound regeneration with bioactive glass-gold nanoparticles ointment, *Biomed. Mater.* 14 (2019), 025011, <https://doi.org/10.1088/1748-605X/aaf7d>.
- [25] T. Kokubo, H. Takadama, How useful is SBF in predicting in vivo bone bioactivity? *Biomater.* 27 (2006) 2907–2915, <https://doi.org/10.1016/j.biomaterials.2006.01.017>.
- [26] K. Magyari, Z.R. Tóth, Z. Pap, E. Licarete, D.C. Vodnar, M. Todea, T. Gyulavári, K. Hernádi, L. Baia, Insights into the effect of gold nanospheres, nanotriangles and spherical nanocages on the structural, morphological and biological properties of bioactive glasses, *J. Non-Cryst. Solids* 522 (2019), 119552, <https://doi.org/10.1016/j.jnoncrsol.2019.119552>.
- [27] D. Inzunza, C. Covarrubias, A. Von Martens, Y. Leighton, J.C. Carvajal, F. Valenzuela, M. Díaz-Dosque, N. Méndez, C. Martínez, A.M. Pino, J.P. Rodríguez, M. Cáceres, P. Smith, Synthesis of nanostructured porous silica coatings on titanium and their cell adhesive and osteogenic differentiation properties, *J. Biomed. Mater. Res. A* 102 (2014) 37–48, <https://doi.org/10.1002/jbm.a.34673>.

